Structure and evolution of the Baikal rift: A synthesis

Carole Petit, Jacques Déverchère

Geochemistry Geophysics Geosystems G3
AN ELECTRONIC JOURNAL OF THE EARTH SCIENCES
Published by AGU and the Geochemical Society

Article
Volume 7, Number 11
21 November 2006
Q11016, doi:10.1029/2006GC001265
ISSN: 1525-2027

Structure and evolution of the Baikal rift: A synthesis

Carole Petit
Laboratoire de Tectonique, Université Pierre et Marie Curie – Paris6, UMR CNRS 7072, Tour 46-00 E2, Boîte 129, 4 Place Jussieu, F-75252 Paris Cedex, France (carole.petit@lgs.jussieu.fr)

Jacques Déverchère
UMR CNRS 6536 Domaines Océaniques, Université de Bretagne Occidentale, Technopôle Brest-Iroise, Place Nicolas Copernic, F-29280 Plouzané, France

[1] Active continental rifts are spectacular manifestations of the deformation of continents but are not very numerous at the surface of the Earth. Among them, the Baikal rift has been extensively studied during the last decades. Yet no simple scenario explains its origin and development because the style of rifting has changed throughout its ~30 Myr history. In this paper, we use forward and inverse models of gravity data to map the Moho and lithosphere-asthenosphere boundary in three dimensions. We then integrate these new results with existing geophysical and geological data on the Baikal rift structure and dynamics, and propose a scenario of its evolution. Earthquake depths, mantle xenoliths, heat flow, and seismic and gravity models advocate for a normal to moderately thinned continental lithosphere and crust, except beneath the Siberian craton, which exhibits a >100-km-thick lithosphere. Relatively thin lithosphere (70–80 km) is found east and south of the rift system and is in spatial connection with the Hangai-Hövsgöl region of anomalous mantle in Mongolia. From top to bottom, the rift structure is asymmetric and appears strongly controlled by the geometry of the suture zone bounding the Siberian craton. Moreover, the mode of topography support changes significantly along the length of the rift: mountain ranges south and north of the rift are underlain by negative Bouguer anomalies, suggesting deep crustal roots and/or anomalous mantle; rift shoulders in the center of the rift seem to result from flexural uplift. The commonly assumed "two-stage" rift evolution is not corroborated by all stratigraphic and seismic data; however, it seems clear that during the Oligocene, an "early stage," which might be dominated by strike-slip tectonics instead of pure extension, created primitive basins much different from the present ones. Most of the "true" rift basins seem to have initiated later, during the Late Miocene or Pliocene. This kinematic change from strike-slip to extensional tectonics in the Baikal rift is part of a more general kinematic reorganization of Asia and can be associated with the rapid growth of the Tibetan plateau and the end of marginal basins opening along the Pacific boundary.

Components: 13,419 words, 15 figures.

Keywords: Baikal; rift; Asia; geodynamics; rheology.

Index Terms: 8002 Structural Geology: Continental neotectonics (8107); 8109 Tectonophysics: Continental tectonics: extensional (0905); 8159 Tectonophysics: Rheology: crust and lithosphere (8031).

Received 1 February 2006; **Revised** 10 July 2006; **Accepted** 8 September 2006; **Published** 21 November 2006.

Petit, C., and J. Déverchère (2006), Structure and evolution of the Baikal rift: A synthesis, *Geochem. Geophys. Geosyst.*, *7*, Q11016, doi:10.1029/2006GC001265.

1. Introduction

[2] Continental extension occurs in a variety of tectonic settings (postorogenic extension, back-arc extension, pull-apart opening, etc.) and results in a large set of tectonic structures [*Ruppel*, 1995]. Besides the geodynamic context, the rheological layering of the lithosphere exerts a first-order control on the rift geometry. According to *Buck* [1991], so-called "wide" or "diffuse" rifts characterize areas of widespread extensional deformation developing within a weak lithosphere, such as the Basin and Range Province or Tibetan Plateau. On the other hand, so-called "narrow" or "discrete" rifts are zones of intense, well-localized deformation in a relatively strong lithosphere and are likely to represent the early stages of continental break-up. The most active of these localized rifts are the East African, Baikal, and Rio Grande. Understanding how such continental rifts form and develop is one of the important stakes of modern tectonics, since it is one of the processes which create new plate boundaries, participating to the deformation of continents.

[3] For several decades, many studies have been devoted to the Baikal Rift System (BRS); its surface tectonics [e.g., *Sankov et al.*, 2000; *Sherman*, 1992; *Sherman et al.*, 2004], present-day kinematics [*Calais et al.*, 1998, 2003], basin sediments [*Hutchinson et al.*, 1992; *Kuzmin et al.*, 2000; *Moore et al.*, 1997; *Nikolaev et al.*, 1985], earthquakes [e.g., *Déverchère et al.*, 1991, 1993; *Doser*, 1991a, 1991b], volcanics [e.g., *Ionov et al.*, 1995; *Kiselev and Popov*, 1992; *Rasskasov et al.*, 2002], and deep structure [e.g., *Brazier and Nyblade*, 2003; *Pavlenkova et al.*, 2002; *Petit et al.*, 1998; *Suvorov et al.*, 2002; *ten Brink and Taylor*, 2002; *Zorin et al.*, 1990, 2002] have given birth to an important number of publications. Yet, as we will show later, it is still the subject of intense debate concerning its evolution, deep structure or origin [*Ivanov*, 2004]. Concerning the origin of the BRS, the two classical hypotheses of "passive" versus "active" rifting [*Sengör and Burke*, 1978] are still debated. On the basis of the interpretation of gravity, deep seismic soundings and tomography models, some authors [e.g., *Gao et al.*, 2003; *Logatchev and Zorin*, 1987; *Windley and Allen*, 1993; *Zorin*, 1981] argue for the existence of a wide asthenospheric diapir reaching the base of the crust beneath the rift axis. On the basis of very similar data, *Tiberi et al.* [2003] find no evidence for an asthenospheric diapir. On the other hand, it has been proposed that the BRS opens as a kind of pull-apart basin in response to compression coming from the India-Asia collision [*Lesne et al.*, 1998; *Molnar and Tapponnier*, 1975; *Petit et al.*, 1996; *Tapponnier and Molnar*, 1979]. Another matter of discussion is the commonly assumed "two-stage" evolution of the rift [*Logatchev and Zorin*, 1987], which has been recently questioned by *ten Brink and Taylor* [2002]. Finally, because of its contrasted topography and gravity signals, the BRS is well-suited to address the question of the long-term strength of the continental lithosphere, which is another recent and hot debate [see, e.g., *McKenzie and Fairhead*, 1997; *Burov and Watts*, 2005]. From the "narrow rift" versus "wide rift" classification of *Buck* [1991], the BRS appears as a very localized deformation ("narrow rift") advocating for a cold, resistant mantle lithosphere.

[4] To summarize, the main questions arising are as follows:

[5] 1. When did the BRS started to develop, and why?

[6] 2. Which were the different stages of its evolution?

[7] 3. What is its present-day deep structure?

[8] 4. How strong is the lithosphere beneath the BRS?

[9] In this paper, we present a synthesis of the available data on the BRS from surface to depth, to provide a global view of the current knowledge of this continental rift system. We propose a balanced version of its origin and development, taking into account the more regional evolution of Asia. Since an important matter of discussion is the deep rift structure, we also propose new maps of the Moho and asthenosphere depths beneath the BRS based on the inversion of gravity and geoid data.

2. General Setting of the Baikal Rift and Prerift History

2.1. Baikal Rift in Asia

[10] The Baikal Rift System is located in northeast Asia, north of the India-Asia collision zone (Figure 1). It extends over ~1500 km in a ~SW-NE direction and is made of several basins of different ages and geometries [e.g., *Logatchev and Florensov*, 1978]. It is prolonged to the NE by the Stanovoy strike-slip zone [*Parfenov et al.*, 1987] which joins the Sea of Okhotsk and Sakhalin deformation zones [e.g., *Fournier et al.*, 1994]. To the SW, it is connected

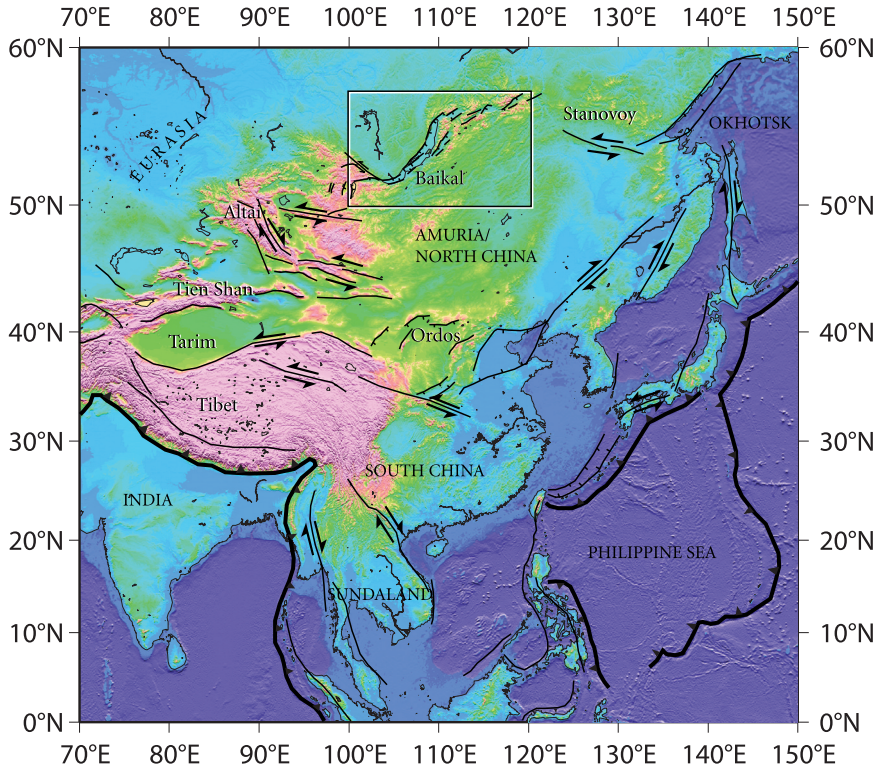

Figure 1. Topographic and neotectonic map of Asia (faults drawn after *Fournier et al.* [2004]). Names in capital letters indicate the main tectonic plates or blocks; inset shows the study region.

to the system of left-lateral strike-slip faults of western Mongolia [e.g., *Cunningham*, 2001]. From a kinematic point of view, the BRS is part of the western boundary of the Amurian (or North China) plate, which moves eastward with respect to Eurasia at a rate of less than 1 cm/yr [e.g., *Calais et al.*, 2003; *Wei and Seno*, 1998; *Zonenshain and Savostin*, 1981]. From its geographical situation, and its kinematics, the BRS appears closely linked to the Asian deformation system. Eastward motion of the Amurian/North China plate with respect to Eurasia, although slower, resembles the "escape" of South China, Tibet, and Sundaland blocks evidenced further south, in response to the indentation of India into Eurasia [e.g., *Avouac and Tapponnier*, 1993; *Calais et al.*, 2003; *Chamot-Rooke and Le Pichon*, 1999]. As we will show later, the birth of the Baikal rift is ~20 Ma younger than the initiation of the Indo-Eurasian collision. However, its kinematic evolution and magmatic history bear close relationships with the regional evolution of Asia.

[11] There is a first difficulty in defining the exact extent of the BRS, especially to the southwest, since it is unclear whether the three N-S trending basins of Mongolia are part of the BRS or rather linked to strike-slip tectonics of Mongolia. In the following sections, we will consider that the Baikal rift system sensu stricto ends at the southwest at the Tunka basin and at the northeast at the Chara basin (Figure 2). This definition encompasses regions where the stress regime is strictly extensional or wrench-extensional (see section 2.3).

[12] The topography of the BRS is contrasted (Figure 2): high mountain ranges are found at the southwestern extremity of the rift (Sayan and Hamar-Daban Mountains) and along the North Baikal Rift (NBR). These ranges are part of the large Yablonovy Mountains which extend from the Mongolian border to the Stanovoy region. The Siberian craton is an area of flat, low topography (~500 m) bounding the southern and central Baikal basins. SE of the rift, the Sayan-Baikal folded zone is composed of elongated, moderately elevated (~1000 m) ranges trending NE-SW. The rift system is composed of a dozen of basins trending successively E-W in the south (Tunka and South Baikal basins), NNE-SSW in the center (Centre Baikal, North Baikal, Barguzin basins) and NE-SW to E-W in the east (Upper Angara, Muyakan, Muya basins). Lake Baikal occupies the central part of the rift (South, Centre and North Baikal basins); the other basins are emerged. The

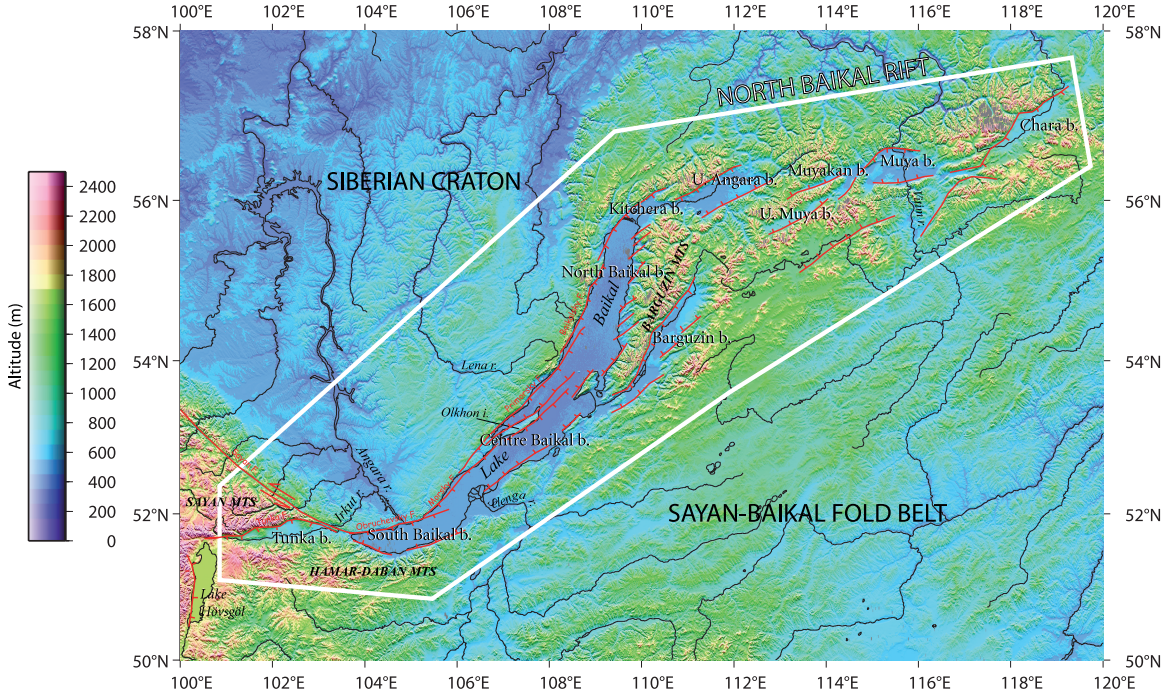

Figure 2. Topography, geography, and main tectonic features of the BRS. Names of the basins are indicated. The white line delineates the inferred spatial extent of the BRS.

drainage is divided into several systems: in the Siberian craton, rivers run toward the North (Angara, Lena), i.e., away from the rift zone. Among them, the Angara River is currently the only outlet of Lake Baikal. It has numerous left tributaries coming from the Sayan Mountains. Lake Baikal itself has ~300 tributaries coming from the North Baikal region (e.g., Upper Angara and Barguzin rivers) and from the high ranges of Western Mongolia (Selenga river) for the largest ones, and smaller ones running down the slope of the narrow rift shoulders, especially along the North Baikal basin. Finally, the Vitim River is the only one which runs through the BRS perpendicular to its strike, across the Muya basin.

2.2. Prerift History

[13] The prerift (i.e., ante-Cenozoic) history of this region is long and complicated since it commenced in the Archaean [e.g., *Delvaux et al.*, 1995; *Ermikov*, 1994; *Melnikov et al.*, 1994; *Zorin*, 1999]. Knowledge of the prerift history is essential to understand how tectonic inheritance controls the modern deformation. Schematically, the lithosphere of the BRS is composed of two adjacent domains of different ages and structures (Figure 3a): (1) the Siberian craton, to the NW, whose basement is Archaean and outcrops SW and NE of the rift zone. It is overlain by a thick Paleozoic and Mesozoic sedimentary cover. Despite its a priori rigid behavior, the crust (or at least its upper layer) has been deformed during Paleozoic and Mesozoic orogenic episodes: the Archaean basement is thrust over the Paleozoic cover north of the Sayan fault, in the Irkutsk region; during the formation of the Baikal-Patom range in the Silurian, numerous thrusts and folds parallel to the border of the craton have deformed the Paleozoic cover on the western side of the rift; (2) the Baikal-Patom range and the Sayan-Baikal fold belt to the east and southeast, which represent respectively the late Proterozoic passive margin of the Siberian craton and an assemblage of micro-continents and volcanic arcs accreted against the craton during the early Paleozoic. Later, during the Mesozoic, the Sayan-Baikal fold belt was reactivated by a continental collision occurring further south along the Mongol-Okhotsk suture. Paleozoic and Mesozoic collisions were followed by postorogenic collapse and granitoid intrusions. These orogenic episodes have given the Sayan-Baikal belt a NE-SW tectonic fabric which is still visible in the topography. The end of the Mesozoic is marked by a phase of tectonic stability and relief planation with creation of a weathering horizon [e.g., *van der Beek et al.*, 1999].

[14] In summary, prerift tectonics resulted in a major weakness zone, the Siberian craton's suture, and in a pervasive NE-SW structural fabric in the

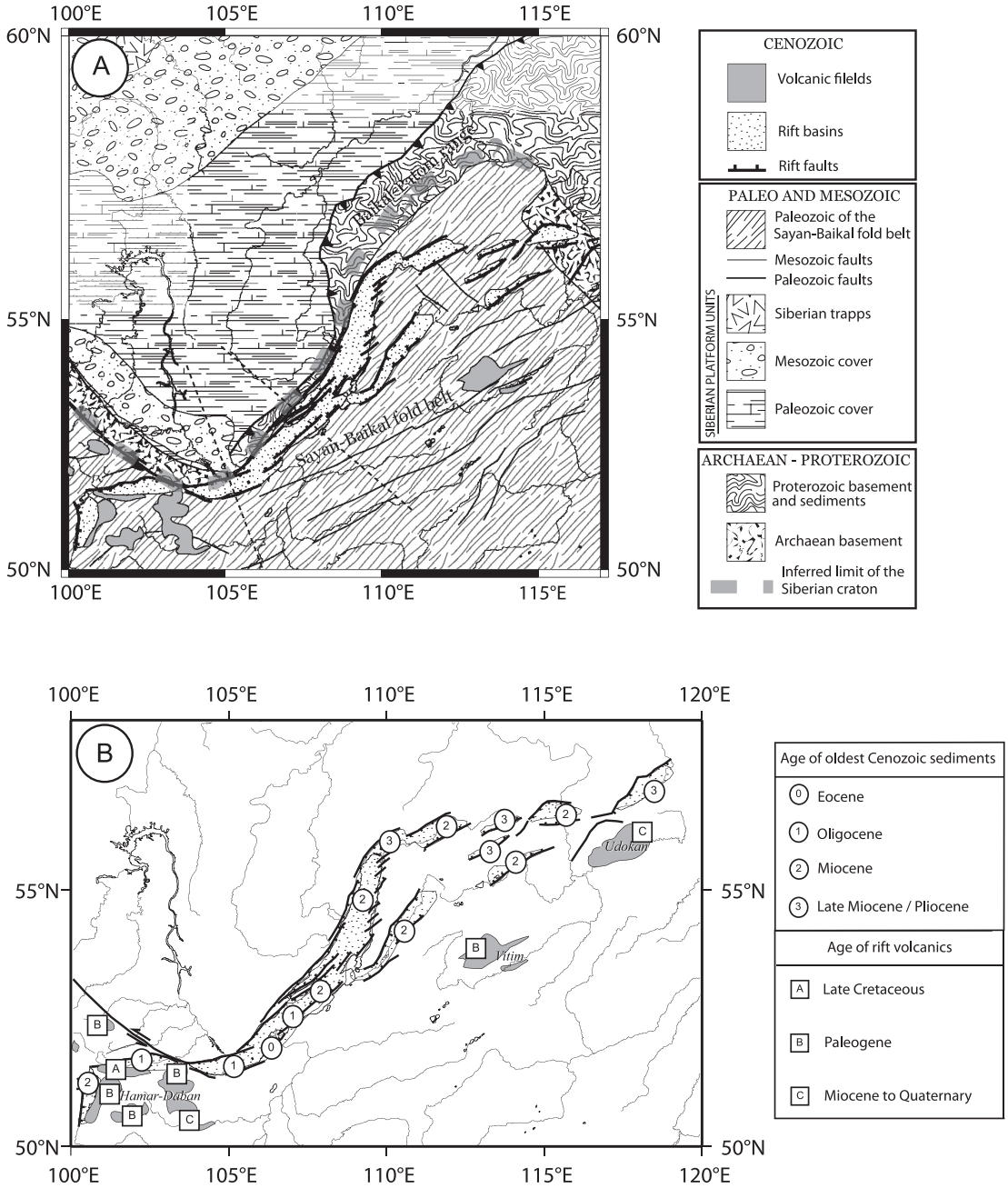

Figure 3. (a) Simplified structural setting of the Baikal Rift System [after *Melnikov et al.*, 1994; *Delvaux et al.*, 1995; *Zorin*, 1999]. (b) Rift basins and volcanics of the BRS. Numbers refer to the inferred age of rift basins; letters indicate the onset of volcanism. Dashed lines show the position of the two cross sections presented in Figure 14.

Sayan-Baikal folded belt. Obviously, this structural inheritance guides the current rift deformation [e.g., *Logatchev and Florensov*, 1978]: the southern half of the rift clearly localizes on the suture, while the north Baikal rift develops within the fold belt and is made of discontinuous en échelon basins trending parallel to the inherited structural grain. However, despite the clear spatial correlation between modern and ancient structures, it is not straightforward to assume that modern normal faults simply branch on ancient thrusts. Indeed, in the center and northern rift areas, the cratonic suture is (or is likely to be) a southeastward flat-dipping fault along which the cratonic crust is underthrust beneath the Sayan-Baikal and Baikal-Patom units [*Delvaux et al.*, 1995]. Therefore steep (60°) and deep (down to ~30 km) normal faults

located vertically above the suture should cut across the cratonic basement at depth.

3. Structures, Strain and Stress Evolution

3.1. Volcanism of the Baikal Rift

[15] Volcanism in the Baikal rift began as early as the Late Cretaceous [*Rasskasov*, 1994], but only in the Tunka basin. As a whole, syn-rift volcanism of the BRS represents ~5000 km^3. The main episode of volcanic activity starts in the Miocene [*Rasskasov et al.*, 2002]; Miocene to quaternary volcanics outcrop: (1) in the western part of the rift, in the Tunka basin and south of it, and in the Hamar-Daban area south of Lake Baikal; (2) southeast of the north Baikal basin, in the Vitim region; and (3) at the extreme northeast of the rift, in the Udokan area (Figure 3b). All but the Tunka basin are devoid of volcanic deposits, since most volcanic centers are located off-axis. Eruptions ceased ~600 ka ago. Lavas are mainly composed of alkaline and subalkaline basalts [*Kiselev et al.*, 1978], with some tholeiitic basalts interbedded with alkaline ones in the Tunka basin. More differentiated lavas of the Hawaiian type (mugearites, benmoreites, and trachytes) are found in the Udokan field. Overall, chemical analyses of basaltic emissions do not evidence any clear evolution in space or time, as could be expected from a progressive erosion of the lithosphere by asthenospheric upwelling [*Kiselev et al.*, 1978]. During the Neogene, similar basaltic eruptions occur as well in Tibet, Mongolia and NE China, suggesting that Baikal rift volcanism is a local manifestation of a more regional volcanic episode affecting the eastern Asian continent [e.g., *Barry et al.*, 2003; *Wang et al.*, 2001]. Trace element, REE and isotopic modeling of Mongolian basalt compositions indicate that the melts formed within the lithospheric mantle, at depths larger than 70 km, from recently metasomatised lithosphere [*Barry et al.*, 2003]. These authors suggest that partial melting can be explained by a low heat flux thermal anomaly, and possibly enhanced by local lithospheric delamination.

3.2. Basin Development

[16] The age of the beginning of rifting is difficult to determine. Sedimentary rocks dated as Late Cretaceous – Eocene on the basis of lithostratigraphic arguments [*Mats*, 1993] are found in the South Baikal and Tunka basins, and likely come from in situ erosion and redeposition of the weathering crust rather than from rifting processes [*Kashik and Masilov*, 1994]. Eocene deposits are locally found around the Selenga delta in the South Baikal basin [e.g., *Scholz and Hutchinson*, 2000]. More widespread deposits typical of shallow basins are dated around ~27 Ma (i.e., in the Late Oligocene) in the South Baikal, Centre Baikal and Tunka basins. Basins of the North Baikal rift initiated later, i.e. mostly in the Pliocene [e.g., *Hutchinson et al.*, 1992] (Figure 4).

[17] Correlation between seismic data and onshore stratigraphy led some authors to divide the sedimentary infill into three main units (Figure 4): a so-called "proto-rift" [*Hutchinson et al.*, 1992] or "early rift" [*Kashik and Masilov*, 1994] unit described in seismic profiles as a made of transparent to discontinuous horizons associated with proximal, shallow-water environments [*Moore et al.*, 1997]. It is often folded and faulted [e.g., *Levi et al.*, 1997]. Its equivalents onshore are the Tankhoy formation on the southern shore of the South Baikal basin, which is a fine-grained coal-bearing molasse, and the Khalagay (Tagay and Sasa) formation (lacustrine clays, siltstones and fine sandstones) on the Olkhon island which is dated by biostratigraphy and paleomagnetism Lower Miocene to Early Pliocene [*Nikolaev et al.*, 1985; *Kashik and Masilov*, 1994; *Mats et al.*, 2000]. The lithology of these deposits suggests an environment of wide, shallow lakes with slow subsidence. They are found around the Tunka, and South and Centre Baikal basins, the latter being now the deepest (up to 9 km of sediments and 1.5 km of water infill) and presumably the oldest. *Moore et al.* [1997] suggest that a thin layer of Miocene sediments exists also in the North Baikal basin, but this is questioned by other authors [e.g., *Hutchinson et al.*, 1992; *Mats et al.*, 2000] who rather propose a Pliocene age for the beginning of sedimentation in this basin. The top of the proto-rift unit is marked for *Hutchinson et al.* [1992] by a transition from transparent to semicontinuous facies. A comparison between different seismic profiles shows that it is correlated with the top of the B3 sequence of *Moore et al.* [1997]. The proto-rift unit correlates well with the high-velocity (3 to 4 km/s) sedimentary layer evidenced on seismic refraction profiles by *ten Brink and Taylor* [2002].

[18] The second main unit is commonly called "middle rift" and is part of the "late-rift" stage, following the terminology of *Hutchinson et al.* [1992] and *Kashik and Masilov* [1994]. It lies with a small angular unconformity on the "proto-rift"

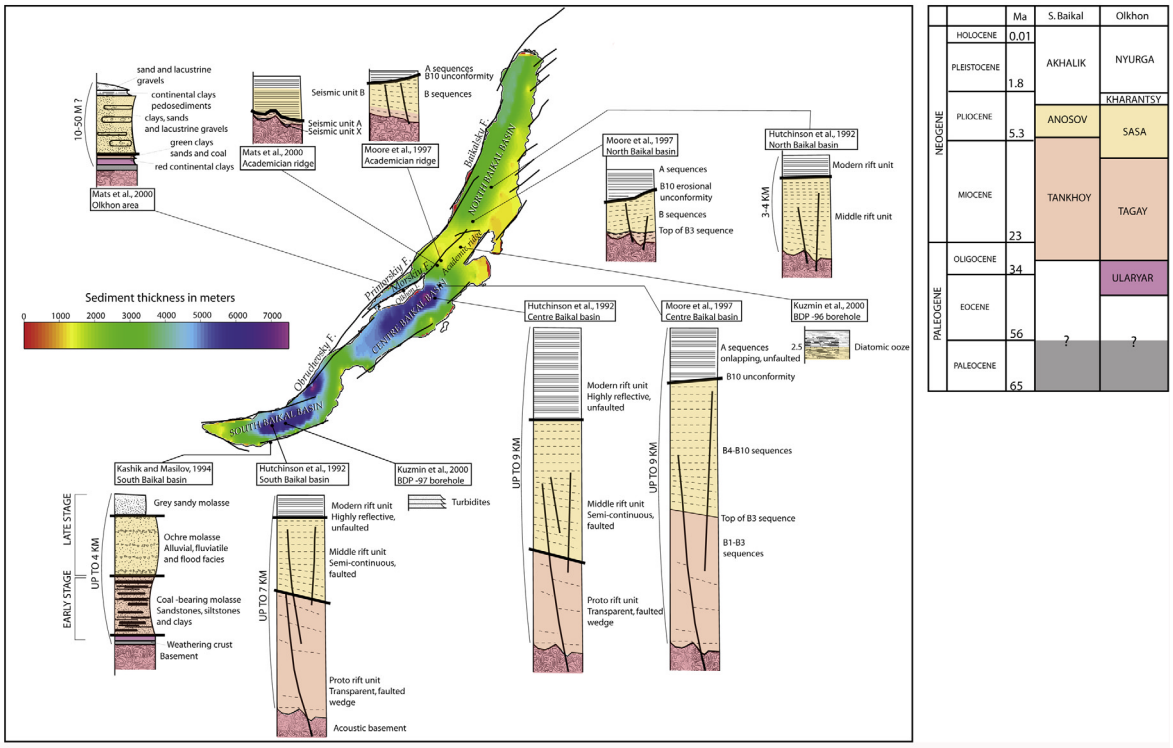

Figure 4. Compilation of sedimentological and seismic data over the Baikal rift (references are indicated). Average thicknesses are indicated on the left of synthetic logs, when available. Right panel indicates the ages of onshore sedimentary units.

unit. It is depicted on seismic profiles by semi-continuous, faulted horizons and is correlated onshore with the Anosov formation. It is made of coarse-grained sandstones and poorly sorted conglomerates and was dated Middle to Upper Pliocene on the basis of its paleontologic content [*Nikolaev et al.*, 1985]. Because of its coarser granulometry, this second unit is generally associated with increasing subsidence and uplift rates. Pliocene sediments are found in almost all rift basins, suggesting that the present-day rift system geometry has been acquired at that time. The transition between proto- and middle-rift sediments was dated at about 4 Ma onshore close to South Baikal basin [*Kashik and Masilov*, 1994] and around 7–10 Ma on the Olkhon Island [*Mats et al.*, 2000]. Actually, *Mats et al.* [2000] suggest that the proto-rift/middle-rift transition is diachronous and starts at the base of the Sasa sequence (Upper Miocene, Figure 4) in the deepest areas, and progressively onlaps on the relief.

[19] Finally, the "modern rift" unit (the latest element of the "late-rift" stage), consists of parallel, continuous reflectors on-lapping on the former (cf. the B10 erosional unconformity of *Moore et al.* [1997]). *Hutchinson et al.* [1992] associate it with the Pleistocene Akhalik formation composed of fluvial, glacial and deltaic sediments. Borehole BDP-97 in the South Baikal basin has revealed that this formation corresponds in the deep lake to a thick series of turbidites [*Kuzmin et al.*, 2000]. The supposed B10 discontinuity has been drilled on the Academician ridge (borehole BDP-96 [*Kuzmin et al.*, 2000]), but no clear erosional discontinuity was evidenced, contrary to the interpretation of *Moore et al.* [1997] in the North Baikal basin. Paleomagnetic datings have associated the middle-rift/modern-rift transition to the Gauss-Matuyama reversal, which gives a Late Pliocene age (~2.6 ± 0.1 Ma) [*Kuzmin et al.*, 2000].

[20] *Logatchev and Zorin* [1987] proposed a "two-stage" rift model with a first, "slow-rifting" stage characterized by low vertical movements, and fine-grained sediments deposited in wide, shallow basins (the "proto-rift" unit), and a second, "fast-rifting" stage corresponding to the two younger units and showing dramatic increases of subsidence and uplift rates, and basins narrowing.

[21] Recently, some authors have questioned this subdivision, on the basis of core-drilling and seismic data covering the Center Baikal basin. *Kuzmin et al.* [2000] have evidenced a continuous, deep-

water hemi-pelagic sedimentation in the Academician ridge for the last 5 Myr, which contradicts the abrupt change in sedimentary environment inferred at around 4 Ma [*Kashik and Masilov*, 1994]. However, because of its sheltered position, sedimentation on the Academician ridge might not record strong regional changes. And, as explained above, the proto-rift/middle rift limit might be older than 5 Ma on the Academician ridge. Seismic refraction data evidence a progressive increase in sediment velocities with depth in the Centre Baikal basin, without any coherent reflective horizon [*ten Brink and Taylor*, 2002]. *Ten Brink and Taylor* [2002] also observe that the transition from transparent to reflective seismic facies crosses seismic horizons, suggesting that it is rather due to diagenetic processes than to original variations of lithology. However, they still observe a 2- to 4-km-thick layer of high-velocity sediments in the Centre Baikal basin, which correlates well with the first rift unit; it is overlain by a layer of low-velocity sediments which likely corresponds to the 2nd and 3rd units.

[22] In summary, despite the difficult correlation between seismic data and interpretations, one can draw the following general history of sedimentation in the Baikal rift:

[23] 1. Sedimentation began during the Cenozoic in and around the South and Center basins and Academician ridge around 27–30 Ma, with fine-grained deposits typical of wide, shallow-water lakes. These sediments might not be related to purely extensional dynamics (see after, stress field evolution).

[24] 2. Around 10–7 and up to 4 Ma, large changes occur in the sedimentary environment of the South Baikal basin and on the Olkhon Island, reflecting increasing subsidence and uplift rates, while sedimentation remains steady in the Centre Baikal basin. The North Baikal basin, and probably the basins of the North Baikal Rift start to develop during this period of time.

[25] 3. From 2.5 Ma to present, another rifting event is documented almost everywhere (except on the Academician ridge) by a pervasive angular and/or erosional unconformity. Changes in the sedimentary environment at this time are also marked by climate fluctuations [e.g., *Back et al.*, 1999].

3.3. Stress Field Evolution

3.3.1. Cenozoic Stress Field

[26] Stress field variations during the Cenozoic rifting history have been detailed by *Delvaux et al.* [1997], on the basis of fault slickensides measured in recent sedimentary formations. These authors have proposed that the "slow-rifting" stage (Oligocene to middle Miocene) was marked by dominantly strike-slip motions with a maximum horizontal stress trending NW-SE around the Tunka basin and NE-SW in the Centre Baikal and Barguzin basins; hence initial rift basins developed along left-lateral faults with a variable normal component, thus questioning the "rift" origin of these primitive basins. This early strike-slip regime is expressed in lake sediments by numerous symmetric folds [*Levi et al.*, 1997].

[27] During the upper Miocene (i.e., around ~10–7 Ma), the stress regime changes from dominant transpression to transtension or pure extension [*Delvaux et al.*, 1997], suggesting a general kinematic reorganization of the whole BRS, probably corresponding to the first change of subsidence and uplift rates recorded in the sedimentary section [*Delvaux et al.*, 1997]. It is worth noting that the Upper Miocene corresponds to major changes in stress conditions around the eastern margins of the Asian continent, with the transition from dominant extension with back-arc basins opening (for example South China, Japan and Okhotsk seas) to purely compressional regime [e.g., *Fournier et al.*, 2004; *Jolivet and Tamaki*, 1992]. Nearly at the same time (i.e., ~8 Ma), strengthening of the Indian monsoon and beginning of buckling in the East Indian ocean [e.g., *Cochran*, 1990; *Harrison et al.*, 1992] are observed, both of which could be linked to a rapid uplift of the Tibetan plateau [*Molnar*, 2005].

3.3.2. Present-Day Stress and Velocity Field

[28] Present-day kinematic and stress field data evidence three main domains: the southwestern rift zone is characterized by a dominant strike-slip regime, with transpression in the extreme southwest (Tunka basin [see *Arjannikova et al.*, 2004; *Delouis et al.*, 2002; *Larroque et al.*, 2001]) and transtension in the northeast (Figures 5a and 5b). The maximum horizontal stress has a constant SW-NE trend. To the west, SW-NE compression causes left-lateral and reverse motions along the border of the Siberian craton, rapidly changing to NW-SE normal faulting in the South Baikal basin [*Calais et al.*, 2003; *Radziminovitch et al.*, 2005]. This transition from compression to extension seems to result from the interaction between far-field (i.e., coming from the India-Asia collision) SW-NE compressional forces and the downward

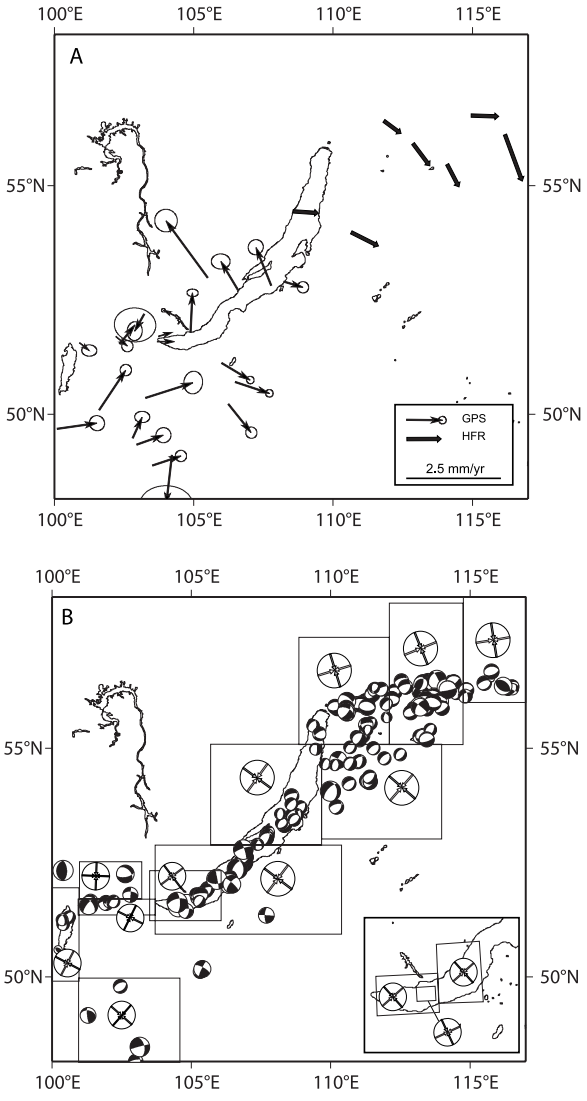

Figure 5. (a) GPS velocities with respect to stable Eurasia (thin arrows) and Holocene fault rates (thick arrows) of the BRS [after *Calais et al.*, 2003; *Sankov et al.*, 2000]. (b) Focal mechanisms and stress field, after the regional study of *Petit et al.* [1996] (large stress symbols) and more detailed studies on the Tunka and South Baikal basins by *Delouis et al.* [2002] and *Radziminovitch et al.* [2005] (small stress symbols and inset). Horizontal principal stresses are indicated as follows: solid arrows, σ_1; gray arrows, σ_2; open arrows, σ_3.

pointing V-shape of the rigid Siberian craton [e.g., *Petit et al.*, 1996]. The Centre Baikal and Barguzin basins show very similar extensional regimes with NW-SE extension and almost no strike-slip focal mechanisms, while the North and southernmost Baikal rift has mixed extensional and left-lateral motions detected on focal mechanisms as well as on finite Holocene displacements on fault scarps [*Doser*, 1991b; *Houdry*, 1994; *Petit et al.*, 1996; *Sankov et al.*, 2000; *Radziminovitch et al.*, 2005]. In summary, the present-day velocity and stress fields of the Baikal rift display changes from pure extension in the rift middle to oblique, left-lateral extension or compression in its southern and northern extremities.

[29] Besides surface manifestations of extensional deformation, another important step toward the understanding of rift evolution is to decipher the deep structure and mechanical behavior of the lithosphere.

4. Mechanical and Thermal Properties of the Lithosphere

4.1. Crustal and Lithospheric Rheologies

[30] Mechanical behavior of the crust and lithosphere primarily depends on its chemical composition and thermal state [e.g., *Burov and Diament*, 1995]. Lithospheric strength will in turn control its response to extension: flexural rebound, fault geometry and seismicity distribution at depth, and so on. Therefore determination of crustal and lithospheric strength variations is of crucial interest to infer the existence of a possible weakness zone due to thermal perturbation.

[31] The rheology of the crust has been investigated through depth distribution of earthquakes [*Déverchère et al.*, 2001]. Precise hypocenter determination has shown that the crust has a brittle behavior, at least at the short timescale of seismic observation, down to at least 30 km. "Deep" earthquakes (25–30 km) are found beneath the Centre and South Baikal basins and in the northern part of the rift [*Déverchère et al.*, 1991]. They can be associated with a strong lower crust with a dominant mafic composition and a "cold" geotherm typical of an 80- to 100-Myr-old lithosphere [*Déverchère et al.*, 2001]. Focal mechanisms of earthquakes are remarkably similar whatever the hypocenter depth, so that there is no evidence for listric faults; this observation does not contradict the possible existence of low-dipping ductile shear zones, as suggested by *ten Brink and Taylor* [2002].

[32] Flexural models based on forward modeling of gravity data have consistently evidenced high effective elastic thickness (Te) values of 30–50 km in the Baikal rift [*Burov et al.*, 1994; *Petit et al.*, 1997; *Ruppel et al.*, 1993; *van der Beek*, 1997]. The Siberian craton appears stronger (Te $\sim$ 60 km) than the Sayan-Baikal belt (Te $\sim$ 30–40 km). Flexural models demonstrate that the lithosphere

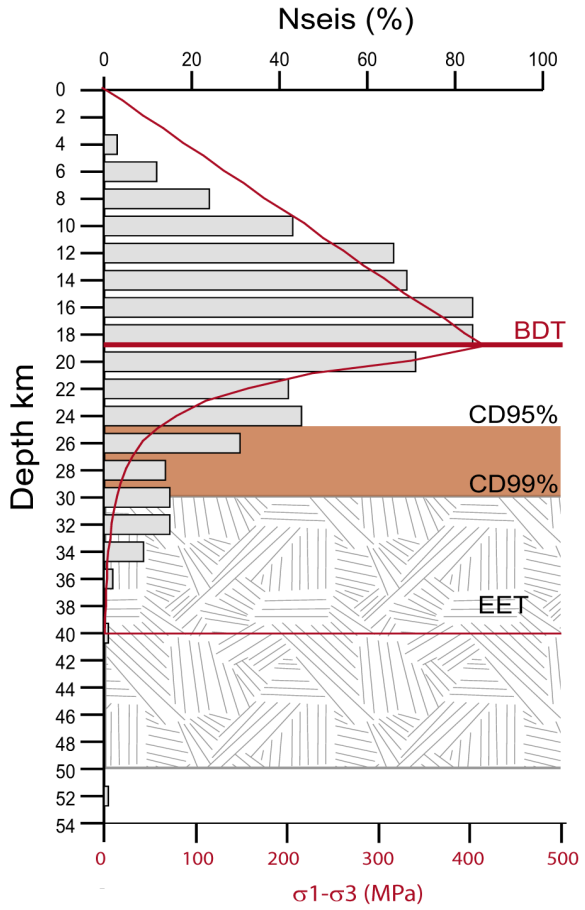

Figure 6. Synthesis of rheological data of the BRS. Histogram shows the depth distribution of earthquakes. Horizontal orange rectangle indicates the 95% and 99% cut-off depths (CD). Red line is the inferred yield strength envelope of the crust [after *Déverchère et al.*, 2001], with its corresponding brittle-ductile transition (BDT). The rectangle delineated by the hash mark pattern covers the range of EET values determined in the BRS from spectral analyses and flexural models [after *Ruppel et al.*, 1993; *Petit et al.*, 1997].

does not behave as a single continuous plate, but that the BRS is a major discontinuity where plate flexure localizes.

[33] Modeled Te values are significantly higher than the thickness of the seismogenic crust, and than the depth of brittle/ductile transition defined by yield stress envelopes (Figure 6); as the effective elastic thickness of the lithosphere reflects the contributions of both crust and mantle elastic lids, we conclude that the lithospheric mantle contributes to a nonnegligible part of the integrated lithospheric strength. Overall, crustal and lithospheric rheologies deduced from earthquake distributions and/or from flexural models advocate for a relatively cold geotherm, not significantly different from those of "stable" continental areas; indeed, a high thermal gradient would result in a much shallower brittle/ductile transition in the crust, and almost entirely ductile lithospheric mantle [e.g., *Burov and Diament*, 1995; *Watts and Burov*, 2003].

[34] The effective elastic thickness controls the flexural response of the lithosphere to topography loads. In a following section, we invert gravity data to retrieve the Moho geometry and use it to determine how the topography is supported, and infer the elastic thickness of the lithosphere.

[35] Another control on the rheology of the lithosphere comes from independent estimates of its thermal state, from direct or indirect measures of the geothermal gradient.

4.2. Thermal and Compositional State of the Lithosphere

4.2.1. Surface Heat Flow

[36] Numerous heat flow measurements in the BRS were previously published [e.g., *Golubev*, 2000; *Lysak*, 1978, 1984] and are available through the worldwide compilation of *Pollack et al.* [1993] at the following ftp address: ftp://ftp.ngdc.noaa.gov/Solid_Earth/Global_Heatflow/. Surface heat flow is remarkably constant and low over the Siberian craton (~40 mW/m^2, Figure 7); it varies between 50 and 60 mW/m^2 in the Sayan-Baikal folded zone, which therefore displays surface heat flow values typical of "stable" continents. Only moderate heating (60–80 mW/m^2) is evidenced at the rift axis. Locally, very high values (0.3 to 35 W/m^2) have been measured, but these are likely to correspond to hydrothermal circulation along major faults [*Poort and Klerkx*, 2004], rather than to conductive heat output. A high regional heat flow anomaly (>150 mW/m^2) is found east of Lake Hövsgöl (Figure 6). Hence, as concluded by *Poort and Klerkx* [2004], conductive heat flow in the BRS does not seem to bear the signal of large-scale lithospheric thinning.

4.2.2. Mantle Xenoliths

[37] Mantle xenoliths sampled in Cenozoic basalts of the Vitim and Hamar-Daban volcanic fields have provided precise constraints on the upper mantle composition and temperatures near the BRS [e.g., *Ashchepkov*, 1991; *Ionov et al.*, 1995; *Ionov*, 2002; *Kiselev and Popov*, 1992]. *Ionov* [2002] used

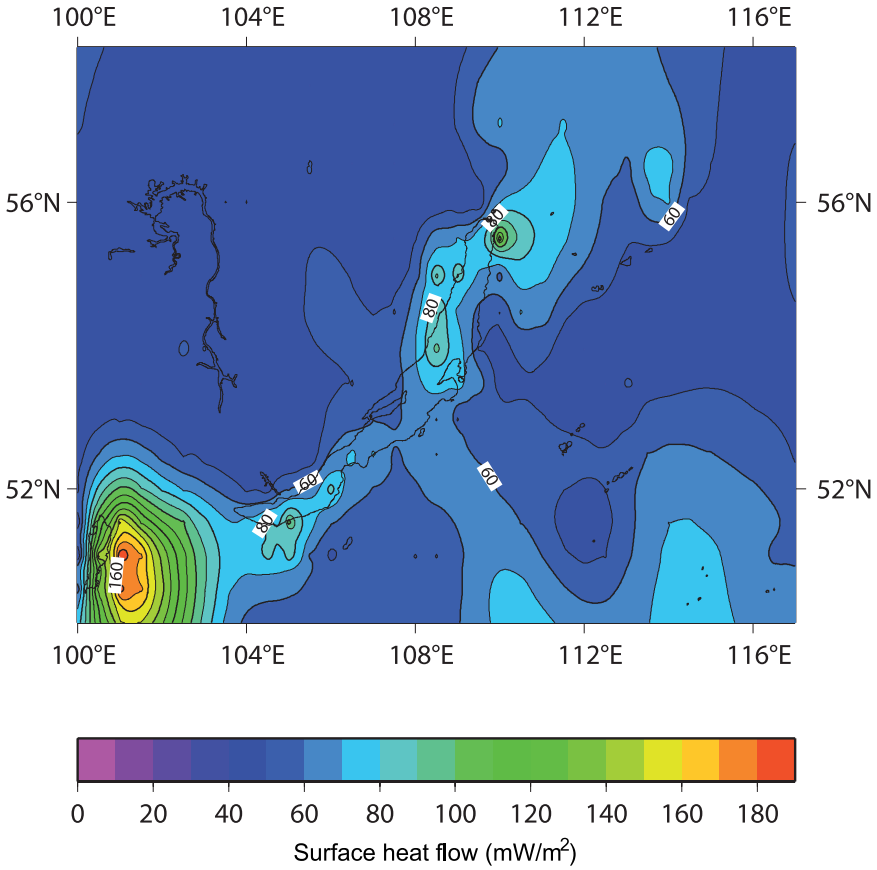

Figure 7. Surface heat flow map of the BRS [after *Pollack et al.*, 1993].

steady state conductive geotherm models to infer that P-T estimates from recent lherzolites of the Vitim volcanic field range along a steady state geotherm characterized by a surface heat flow of 75–90 mW/m^2, which is higher than measured values of 50–60 mW/m^2 (see above) and could reflect recent heating of the upper mantle. In addition, *Ionov* [2002] showed that Miocene xenoliths are colder than Pleistocene ones, indicating a temperature elevation of ~100°C since the Miocene. Steady state thermal models assume that the geotherm has reached its equilibrium, i.e. that the last thermal event is old (i.e., 100 Ma or more). When comparing xenolith data to a cooling-plate model, it appears that Miocene xenoliths are indeed close to the steady state geotherm for the cooling-plate model with a cooling age of ~80 Ma and a characteristic surface heat flow of 50–55 mW/m^2, whereas Pleistocene xenoliths advocate for an unsteady geotherm (Figure 8). Following *Ionov*'s [2002] hypothesis of recent (~2 Ma) heating of the base of the lithosphere (i.e., replacement of lithospheric mantle by asthenosphere with a constant temperature of 1300°C), a cooling-plate model satisfyingly fits Pleistocene temperatures for an uplift of the lithosphere-asthenosphere boundary (LAB) up to 65–70 km (Figure 8). Therefore it is possible that P-T paths from recent xenoliths exhibit steeper PT slopes than equilibrium geotherms simply because the lithosphere is still cooling from a recent thermal event.

[38] In general, P-T paths from recent xenoliths show that the lithosphere (defined as the depth to the 1300° isotherm) remains more than 70 km thick [e.g., *Ionov et al.*, 1995; *Kiselev and Popov*, 1992] (Figure 8), thus ruling out the existence of an asthenospheric upwarp rising up to 50 km, as suggested by *Gao et al.* [2003]. It is worth noting that xenolith suites come from volcanic fields located off the rift axis. Therefore they do not provide any information on the thermal state of the mantle just beneath the rift. However, the conspicuous absence of volcanism at the rift axis, as well as the abrupt drop of volcanic activity during the Quaternary argues against the presence of an active, shallow-seated asthenospheric upwarp. Xenoliths from the Hamar-Daban (south Baikal) region have similar P-T values as those of the Vitim field, except that no recent heating is

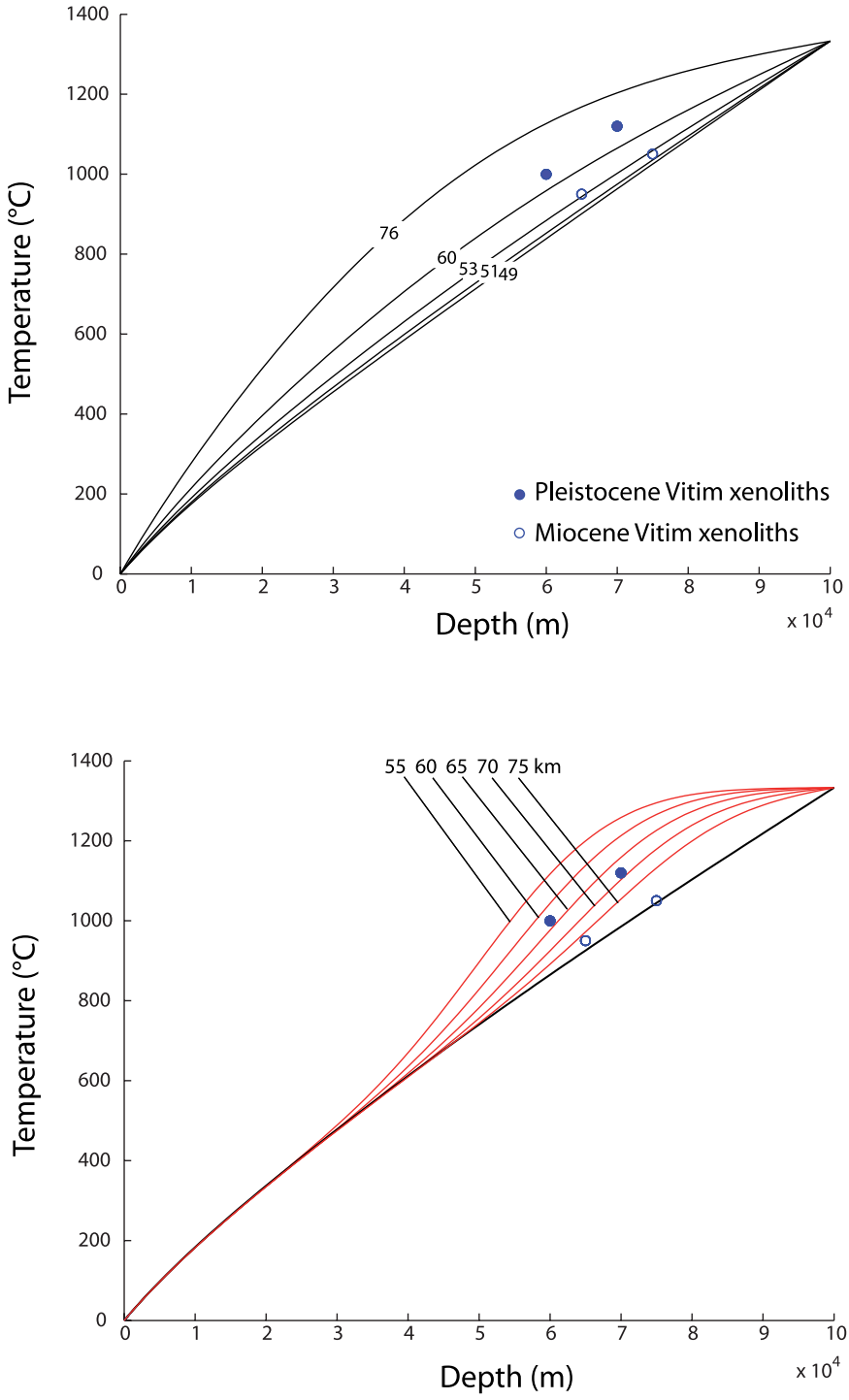

Figure 8. Comparison of P-T data from Miocene (solid blue circles) and Pleistocene (open blue circles) xenoliths, after *Ionov* [2002] with classical cooling plate model temperatures. (top) Cooling-plate geotherms for thermal ages of 20, 40, 60, 80, and 100 Ma (solid lines) with associated surface heat flow (numbers on the curves) in mW/m^2. (bottom) Geotherm after recent (2 Ma) uplift of the lithosphere-asthenosphere boundary of 55, 60, 65, 70, and 75 km, with respect to the 80 Ma geotherm of the top panel (black solid line).

evidenced. In summary, mantle xenoliths advocate for a thick (70 km or more) continental lithosphere overlying a weak, deep-seated positive thermal anomaly located off-axis. To this respect, xenoliths of the BRS are quite similar to those found on the Hangai dome of Mongolia where a deep-seated velocity and gravity anomaly has been evidenced [*Ionov*, 2002; *Petit et al.*, 2002].

4.3. Deep Structures

4.3.1. Crust Geometry

[39] Deep seismic soundings and local tomography have evidenced a crustal thickness of 40–43 km beneath the Siberian craton [e.g., *Pavlenkova et al.*, 2002; *Suvorov et al.*, 2002; *Zorin et al.*, 2002], with relatively high P-velocities (6.9 km/s) in the lower crust. The Sayan-Baikal folded zone seems characterized by a thicker crust (45–50 km) and stronger variations. In particular, the crustal thickness east of Lake Baikal, in the Tunka-Sayan region, reaches more than 50 km, implying a ~10-km step at the Moho across the Sayan fault. Some authors suggest the Moho upwarps up to ~35 km beneath the Centre Baikal basin, implying an uplift of 5–10 km [*Pavlenkova et al.*, 2002; *Suvorov et al.*, 2002; *Zorin et al.*, 2002], while others conclude to a small Moho uplift of less than 3 km [*ten Brink and Taylor*, 2002].

[40] The amount of Moho upwarp depends on the mechanism of extension and compensation: for example, following the necking model of *Kooi et al.* [1992], the relative amounts of surface extension (basin depression) and lower crustal extension (Moho upwarp) will depend on the position of a neutral surface (in a purely kinematic, nonisostatic sense) called "necking level." If this necking level is deep, extension will result in a large surface depression and small Moho upwarp, leading to a net unloading of the lithosphere and subsequent isostatic rebound, while a shallow necking level will result in a positive loading of the lithosphere, and subsidence. In the Centre Baikal basin, this kind of modeling has revealed a deep level of necking [*van der Beek*, 1997] and suggests that the Moho is not strongly upwarped (~3 km).

[41] Considering a simple local isostasy model, with mean altitudes of 600 m for the Siberian craton and 1200 m for the Sayan-Baikal folded zone, and densities for the crust and mantle of 2.67 and 3.2, it follows that a 40-km-deep Moho beneath the craton is in isostatic equilibrium with a 44-km-thick crust beneath the fold zone. Beneath the Centre Baikal basins, assuming 1 km of water and 9 km of sedimentary infill (densities 1.0 and 2.4, respectively) yields a total crustal thickness of about 32 km. However, as we will show later, this computation only provides a proxy for the actual crustal thickness, as significant deviations from local isostasy are likely to occur [*Petit et al.*, 1997; *van der Beek*, 1997].

[42] In a recent paper, *Gao et al.* [2004] published Moho depth estimates based on receiver functions, along a NNW-SSE profile crossing the South Baikal basin. Their results seem to evidence high variations of the crustal thickness, which ranges from 38 to 44 km in the Siberian craton, from 43 to 50 km beneath the Sayan-Baikal folded zone, and decreases to 35 at the rift axis. It is worth noting that their results depend strongly on the assumed crustal velocity and a chosen constant Vp/Vs ratio; for instance, the authors report that a variation of 5% in the assumed crustal velocity would result in a difference of 2 km in the Moho depth. Considering that 5% is a reasonable estimate for the maximum possible velocity variations, the results of *Gao et al.* [2004] are compatible with previously published Moho depth estimates.

[43] To summarize, there is a general agreement on the average estimates of crustal thickness beneath the craton (~40 km) and the fold belt (~45 km), but the Moho depth beneath the rift remains controversial.

4.3.2. Lithosphere Geometry

[44] Numerous global and regional tomography models can be used to draw the general features of mantle anomalies beneath Asia [e.g., *Shapiro and Ritzwoller*, 2002; *Villaseñor et al.*, 2001; *Wu et al.*, 1997; *Yanovskaya and Kozhevnikov*, 2003]. With a varying accuracy, all models image negative velocity anomalies in the mantle above the Hangai dome in western Mongolia, sometimes extending, with lower amplitude, to the Baikal rift axis. High positive velocity anomalies characterize the Siberian craton's mantle. Local tomography models are also abundant over the BRS [e.g., *Brazier and Nyblade*, 2003; *Gao et al.*, 2003; *Petit et al.*, 1998; *Tiberi et al.*, 2003]. Surprisingly, their interpretations show stronger divergences than those of regional and global models. *Gao et al.* [2003] and *Tiberi et al.* [2003] used very similar data: ~1500 delay times of teleseismic earthquakes from a seismic experiment that took place in 1992, and Bouguer gravity data. Whereas *Tiberi et al.* [2003] performed a coupled gravity/tomography inversion using no a priori constraints on density or velocity variations, *Gao et al.* [2003] assumed that travel-time residuals come mostly from depth variations of LAB, and then compared their results with Bouguer gravity data. At lithospheric depths of 100–150 km, both studies show similar results (Figure 9) and evidence a low-velocity mantle beneath the Baikal rift adjacent to a cold, fast mantle beneath the Siberian craton. Yet, while

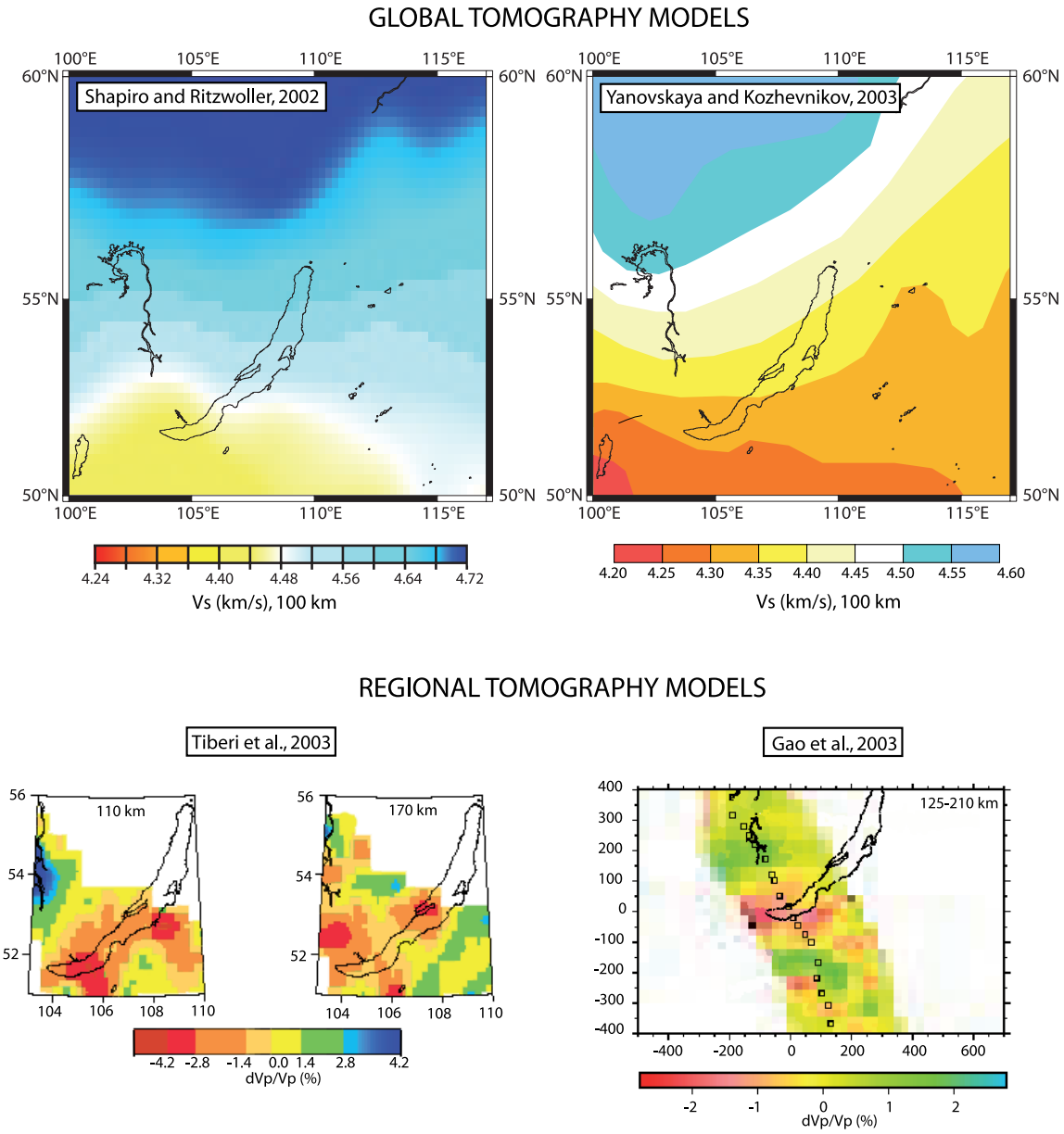

Figure 9. Comparison of tomographic models over the BRS. (top) S-wave velocity at 100 km from Rayleigh wave tomography, redrawn after *Shapiro and Ritzwoller* [2002] (left) and *Yanovskaya and Kozhevnikov* [2003] (right). (bottom) P wave velocity around 150 km from local tomography models, redrawn after *Tiberi et al.* [2003] (left) and *Gao et al.* [2003] (right).

Tiberi et al. [2003] conclude to a deep-seated (70 km or more) negative mantle anomaly, *Gao et al.* [2003] suggest that the LAB reaches the base of the crust (i.e., ~40 km). One should note that *Gao et al.* [2003] consider a constant crustal thickness, even though they suggested later [*Gao et al.*, 2004] that it can vary a lot (see section 4.3.1). The teleseismic profile used by *Gao et al.* [2003] crosses a region (the South Baikal basin) where, as we will show later, the Bouguer gravity anomaly shows high amplitude and short wavelength peaks suggesting undulations in the Moho topography and/or intracrustal density variations. Indeed, the low/high Bouguer gravity observed over the South Baikal basin and Hamar-Daban range, respectively, correlate very well with the positive/negative traveltime residuals observed by *Gao et al.* [2003] at these places. Thus the combined interpretation of gravity and tomography shows that crustal thickness variations have a significant influence on the observed traveltime residuals, though they are generally not well resolved.

[45] Moho and LAB interfaces are characterized by large positive and small negative density contrasts, respectively. Depth variations of these interfaces thus have an effect on measured gravity anomalies. Moreover, they are generally located at different depths so that the wavelength of their signature in the gravity field is different. Provided independent constraints on the mean depth and density contrasts of these interfaces are available, gravity data can be used to invert their 3-D geometry over the whole rift zone.

4.4. Moho and LAB Depth Estimates From Bouguer Gravity Data

4.4.1. Gravity and Geoid Data

[46] A Bouguer gravity map of the BRS was previously published by *Petit et al.* [1997]. Bouguer anomaly is computed from free-air gravity using a density of 2.67 10^3 kg/m^3 for surface topography and includes terrain corrections (Figure 10). Correction for the water and sedimentary infill was made using sediment thickness maps of *Hutchinson et al.* [1992] and *Logatchev and Zorin* [1992] and bathymetric charts of the *INTAS Project 99-1669 Team* [2002] using 1.0 10^3 kg/m^3 and 2.4 10^3 kg/m^3 as mean values of water and sediment densities, respectively. The geoid height was computed from free-air gravity using the algorithm included in the Generic Mapping Tools package [*Wessel and Smith*, 1991] (Figure 10). Finally, isostatic anomalies are computed as the difference between the observed Bouguer gravity and the one computed from a local compensation (in the Airy sense) of topography, water and sediment loads using the same densities as for Bouguer calculation (Figure 10). Positive isostatic anomalies indicate under-compensation, corresponding to a mass excess with respect to the Airy model. Similarly, negative anomalies correspond to a mass deficit.

[47] Isostatic anomalies were computed using a local isostasy hypothesis in order to evidence the presence of uncompensated loads which can result from plate flexure. Regional support tends to produce wider and shallower crustal roots; therefore the isostatic anomalies computed with a local isostasy model should reveal undercompensation, or mass excess, beneath mountain ranges.

[48] Bouguer gravity is, as expected, partly correlated with the topography: the flat Siberian craton is characterized by a remarkably constant Bouguer anomaly of ~ -60 mGal, whereas high amplitude ($\sim$100 mGal) variations are observed in the Sayan-Baikal fold zone. The North Baikal Rift as well as the Sayan Mountains, two regions of elevated topography, are characterized by low Bouguer gravity anomalies. In contrast, it is worth noting that part of the Hamar-Daban range, as well as rift shoulders surrounding the Centre Baikal basins are underlined by relatively high Bouguer gravity anomalies. Finally, only the Centre Baikal basin exhibits a positive Bouguer gravity anomaly, possibly resulting from lower crustal thinning.

[49] Observed geoid heights show a wide path of relatively low values (0 to -20 m) cross-cutting the BRS in a NW-SE direction (Figure 10). Positive values are encountered at the SW and NE tips of the BRS. The observed low geoid over the BRS is not compatible with the classical signature of an active mantle plume like in Yellowstone or Afar, for example. Indeed, the ascent of plume material generally causes dynamic uplift which results in positive geoid anomalies, as the dynamic effect overcomes the density deficit due to the intrusion of plume material.

[50] Over the Siberian craton, the mean isostatic anomaly is zero, suggesting local compensation of the topography. Positive anomalies are found along the western border of the craton, north of the Sayan Mountains. Along Lake Baikal, isostatic anomalies are mostly negative, suggesting that rift shoulders are supported by a deep crustal root. Only small positive anomalies surround the Centre (especially eastern) Baikal basin. Finally, the South Baikal region exhibits high amplitude anomalies, with a large mass deficit over the South Baikal basin and a large mass excess south of it, in the Hamar-Daban range.

4.4.2. Modeling of the Moho and Lithosphere-Asthenosphere Boundary

[51] We determine the geometry of the Moho and lithosphere-asthenosphere interfaces using band-filtering and downward continuation of Bouguer gravity data, assuming that the Bouguer gravity anomaly primarily depends on the undulations of these interfaces, such as

$$\Delta g(k) = 2\pi G\left[(\rho_m - \rho_c)Y(k)e^{-kd} + (\rho_a - \rho_m)Z(k)e^{-kl}\right] \quad (1)$$

where Δg is the Bouguer gravity anomaly in the spectral domain, k is the wave number in km^{-1}, Y and Z are Moho and LAB depth variations respectively, d and l are the mean depths of these interfaces and ρ_m, ρ_c and ρ_a are the densities of the

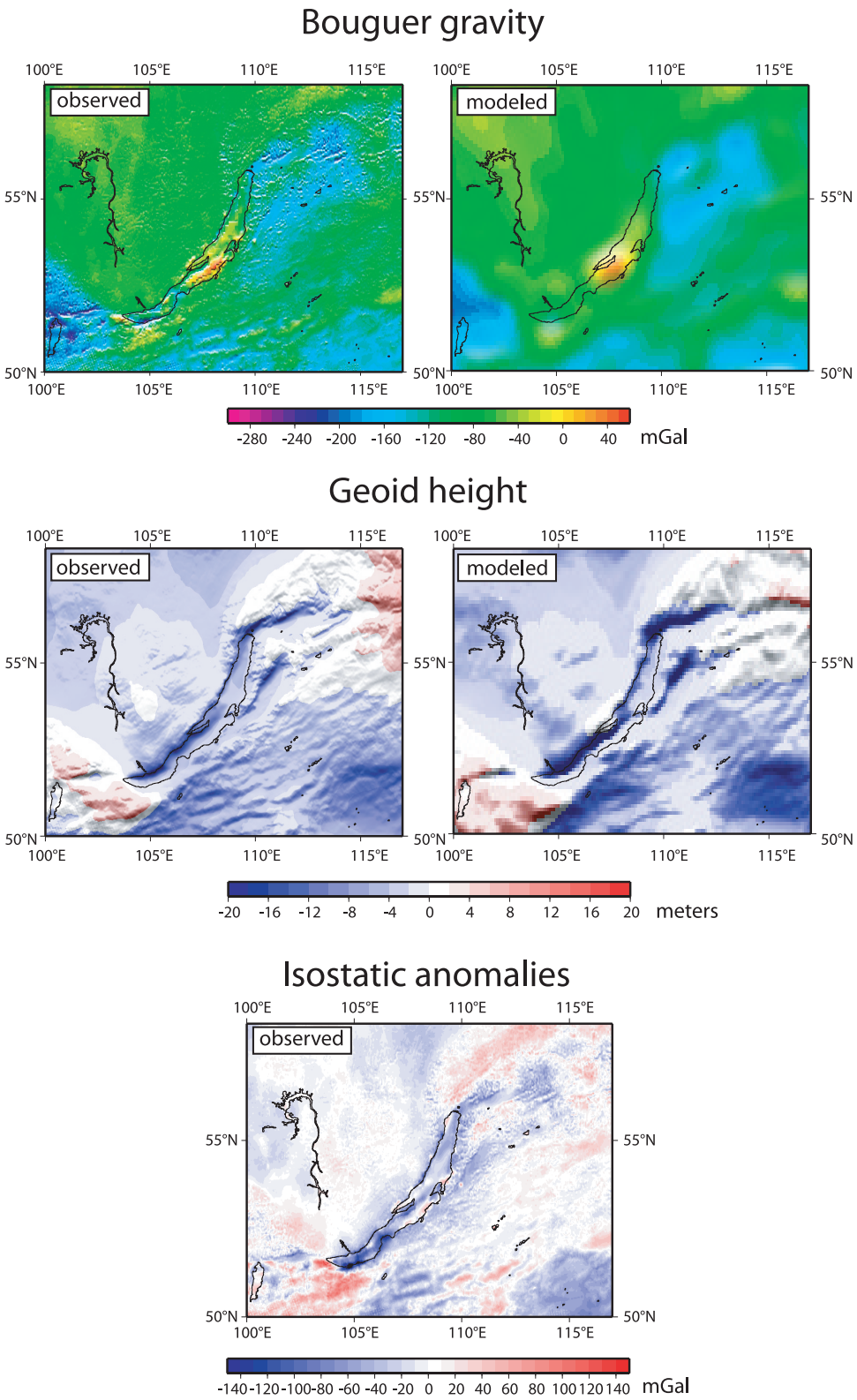

Figure 10. Gravity and geoid data and models over the BRS. Left and right panels correspond to observed and modeled values, respectively. (top) Bouguer gravity redrawn from a compilation of local data already published by *Petit et al.* [1997]. (middle) Relative geoid height, computed as the integral of the gravity field. (bottom) Isostatic anomalies, defined as the difference between observed Bouguer gravity and the one predicted by a local compensation model.

crust, mantle lithosphere and asthenosphere respectively. Since these densities do not vary laterally or vertically for a given layer in our models, any true density contrast within the crust, mantle or asthenosphere will be interpreted as a relief on one or both interfaces. Given the lack of constraints on density variations within the crust, the inversion thus probably overestimates the actual relief of Moho and LAB interfaces. These simple models do not aim at accurately predicting absolute depths to the LAB, as constraints are few, and observations for comparison coarse. Instead, we aim to simulate a possible topography at the LAB and compare the corresponding density contrast and maximum amplitude with tomographic models.

[52] As the determination of source depths and densities from gravity is nonunique, we need to constrain the solution with independent estimates from tomography, xenoliths, and deep seismic soundings. After inversion, the main features of gravity, geoid and isostatic anomalies are generally well retrieved, except for short wavelengths which are more likely to result from intracrustal density variations (Figure 10). In order to separate the effects of Moho and lithosphere-asthenosphere interfaces, we must consider that they are located at different mean depths and thus produce different characteristic wavelengths in the Bouguer gravity signal.

[53] First, we assume that Moho depth variations should produce wavelengths in the Bouguer gravity not smaller than 50–100 km (assuming a mean Moho depth around 30–40 km and a minimum wavelength of Moho undulations similar to the surface width of the rift, i.e., 50 km) and not larger than 900–1000 km (the widest possible source of Moho depth variations arises from differences of crustal thickness between the Siberian craton and Sayan-Baikal folded zone, but this corresponds to a wavelength of 600–700 km). Thus the Bouguer gravity grid was filtered to eliminate short (<100 km) and long (>1000 km) wavelengths which should have more surficial (i.e., intracrustal) or deep (i.e., lithospheric and asthenospheric) sources, respectively. Filtered Bouguer data were then downward continued to a depth d = 28 km (i.e., above the highest supposed Moho) and converted into relative Moho topography in meters using (1). Downward continuation increases the amplitude of the signal and sharpens its edges; therefore it is very sensitive to high-frequency noise. To remove artifacts, we cut high-frequency (i.e., wavelengths smaller than 20 km) peaks by using a low-pass filter; clearly, this filtering limits the benefit of downward continuation by smoothing the signal, but remains acceptable for studying the large-scale Moho geometry of the rift system.

[54] Tests on the density contrast and mean Moho depth were made to find the best agreement with other data. Increasing the density contrast reduces the amplitude of Moho ups and downs. We use as an output constraint a mean Moho depth beneath the Siberian craton of 42 ± 2 km [e.g., *Pavlenkova et al.*, 2002], and test density contrasts at the Moho of 350 kg/m^3, 550 kg/m^3 and 750 kg/m^3 in order to assess the effect of lateral density variations on Moho depth estimates. The resulting minimum Moho depth, encountered over the Centre Baikal basin only, is of 32 ± 5 km (Figure 11). Given the uncertainties, this mean value is comparable to minimum estimates of the crustal thickness beneath the Centre Baikal basin [*Gao et al.*, 2004; *Yanovskaya and Kozhevnikov*, 2003; *Zorin et al.*, 2002] but about 8 km lower than the estimate given by *ten Brink and Taylor* [2002]. The discrepancy between our result and those of ten Brink and Taylor can arise from (1) the use of too large sediment correction in this study or (2) a positive density anomaly in the crust that we did not take into account. Hypothesis 1 is unlikely since sediment correction does not have such dramatic effects in the South and North Baikal basins where the sedimentary thickness reaches 7 km and 3–4 km, respectively, and Moho depth estimates in other places are consistent with seismic and xenolith data. On the other hand, gravity and seismic velocity inversions [*ten Brink and Taylor*, 2002; *Tiberi et al.*, 2003] have already evidenced a high-density, high-velocity crust at this place, thus hypothesis 2 may indeed stand. An anomalous high density (+230 kg/m^3) body at the base of the crust of 5 to 10 km thickness would account for an excess Bouguer gravity with respect to the surrounding regions of ~40 to 80 mGal, which is less than observed (170 mGal). With such a 10-km thick crustal underplating, the remaining 90 mGal can be explained by an uplifted Moho of ~4 km relative to the Siberian Craton, raising the crustal thickness to 36–38 km instead of 32. Taking into account this probably denser lower crust, the value of 32 km computed in this study can therefore underestimate the crustal thickness beneath the Centre Baikal basin by 4 to 6 km. A similar problem arises over the Hamar-Daban range south of Lake Baikal where the crust appears thinned down to 36 ± 4 km precisely beneath the topographic range. Here again, in the lack of other

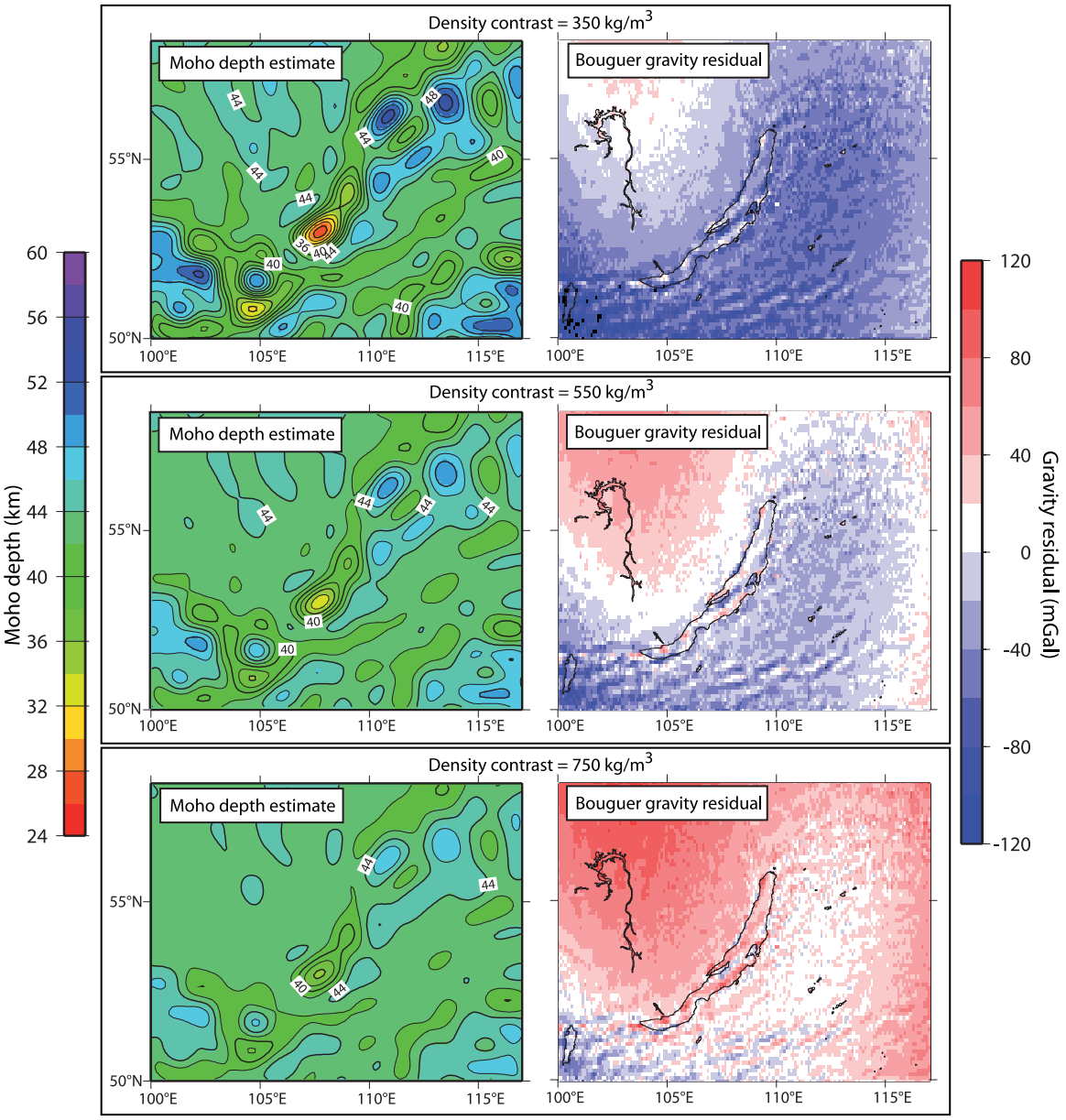

Figure 11. Moho depth estimates from inversion of Bouguer gravity data, using density contrasts at the Moho of (top) 350, (middle) 550, and (bottom) 750 kg.m^{-3}. Left and right panels show the inverted Moho depths and Bouguer gravity residuals, respectively.

constraints on possible density variations within the crust, we may conclude that our estimate provides a lower bound for the actual Moho depth at this place.

[55] The synthetic Bouguer gravity obtained from Moho depth variations is then substracted from the original data. The residual Bouguer gravity is composed of short-wavelengths due to intracrustal loads and data noise, and long wavelengths which can be associated with fluctuations of the lithosphere-asthenosphere boundary (Figure 11, right panel). The gravity grid was extrapolated over ~400 km on its sides in order to avoid side effects during the FFT processing, and a low-pass filter was applied to remove the short wavelengths. Conversion into meters was performed using density contrasts of 20, 30 and 40 kg/m^3 and a downward continuation with l = 60 km (Figure 12). We use as an output constraint minimum and maximum depths of the lithosphere-asthenosphere boundary of 70 and 200 km, respectively. With a low density contrast of 20 kg/m^3, the amplitude of lithosphere-

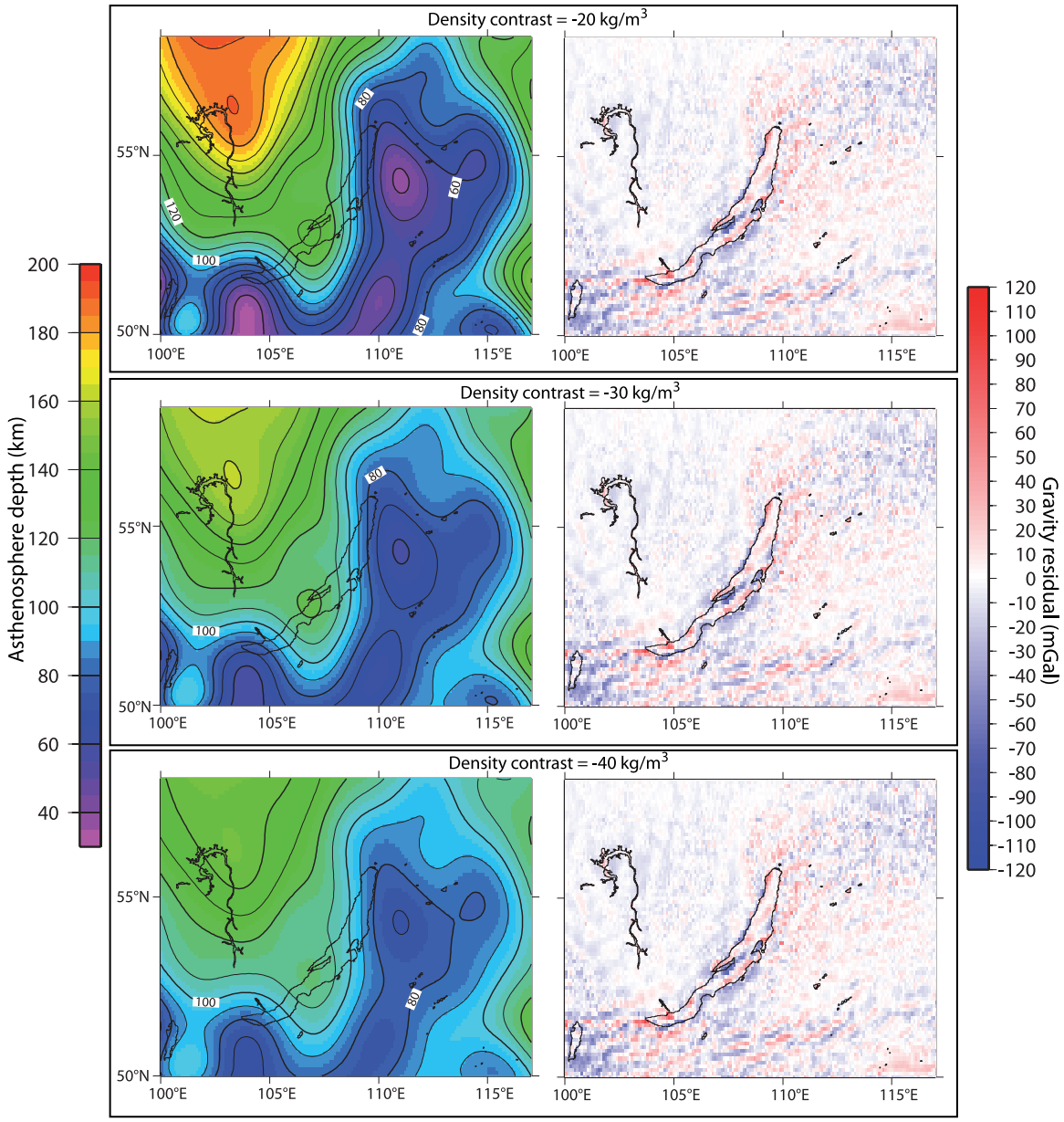

Figure 12. Depth of the lithosphere-asthenosphere boundary estimated from the inversion of long-wavelength gravity residuals shown in Figure 11 (with a density contrast at the Moho of 550 kg.m^{-3}) using a density contrast at the lithosphere-asthenosphere boundary of (top) −20, (middle) −30, and (top) −40 kg.m^{-3}. Left and right panels show the inverted asthenosphere depths and Bouguer gravity residuals, respectively.

asthenosphere boundary topography is much too large (from 40 km to 200 km); the results obtained for 30 kg/m^3 and 40 kg/m^3 provide more realistic estimates.

[56] The resulting lithosphere-asthenosphere boundary is shallowest beneath the Hamar-Daban and Vitim areas (∼70 km), precisely beneath volcanic fields. No significant lithospheric thinning is found at the rift axis. Instead, the lithosphere progressively thickens toward the NW, reaching ∼180 km beneath the core of the Siberian craton. It is worth noting that the area of thinned lithosphere wraps around the rim of the craton, suggesting that anomalous mantle may be channeled along the craton because of the thermal contrast between the craton and its borders [e.g., *Sleep*, 1996].

4.5. Forward Modeling of the Topography

[57] A forward modeling of the topography predicted by the Moho and lithosphere-asthenosphere

topographies can be used to quantify the mean effective elastic thickness. Through this test, we assume that the surface topography loads the Moho and the top of the asthenosphere, resulting in the flexure of a supposed continuous plate, therefore we neglect here effects of plate discontinuity that are indeed believed to occur at the rift axis [e.g., *Petit et al.*, 1997]. We use a finite difference formulation of the general 1-D flexure equation to predict the topography:

$$D\frac{\partial^4 w}{\partial x^4} + \left(\rho_m - \rho_f\right)gw = q$$

where ρ_m and ρ_f are mantle and infill densities, w is the plate flexure, q the plate loading and D is the flexural rigidity depending on the effective elastic thickness (EET) such as

$$D = \frac{E.EET^3}{12(1-\nu^2)}$$

where E is the Young's modulus and ν the Poisson's ratio. We treat separately Moho and asthenosphere contributions by assuming that the Moho geometry represents the flexural response $w1$ to topographic loading $q1$, whereas the variations of the depth of the asthenosphere geometry act as a buried load $q2$ causing a flexural response in the topography $w2$. The total predicted topography corresponds to the sum of Moho- and asthenosphere-supported loads. Geographic coordinates were converted into kilometers and sampled with a grid spacing of 10 km. The Moho topography was smoothed in order to avoid the development of high-frequency peaks due to the 4th order derivation of the deflection. Figure 13 shows the results of topographic modeling for two NW-SE profiles with EET values of 0 (Airy case) 15, 25 and 35 km. The influence of sedimentary and water loads is not taken into account. A small EET value of 15 km renders the plate unable to sustain high topographic loads – compared to the modeled Moho geometry, therefore the supported topography in this case is only of ±250 m. On the contrary, a rigid plate with EET = 35 km is able to support high topographic loads ranging between −1500 and +2000 m, which is higher than observed. A good agreement on topographic amplitudes is found for EET = 25 ± 5 km.

[58] The asthenosphere contribution is not very sensitive to EET variations, because the characteristic wavelengths of asthenosphere topography are too large to be damped by the flexural response of the lithosphere. Therefore the modeled observed variations of topography when changing to EET are principally caused by fluctuations of the Moho interface: high frequency, high amplitude peaks appear because of the high order of the space derivative and increase in height when EET increases. As explained above, this computed topography does not necessarily represent a "true" topography, but rather characteristic wavelengths and amplitudes that could be supported by the plate rigidity. Since the modeled amplitudes in Moho topography are probably over-estimated because we neglected lateral density variations, we suggest that the EET value of 25 ± 5 km provides a lower bound of the true plate rigidity.

5. Conclusion: General Rift Structure and Evolution

5.1. Present-Day Rift Structure

[59] Gravity modeling of deep interfaces has evidenced a varying degree of asymmetry in the rift architecture: minimum crustal thickness is found beneath the Centre Baikal basin (although the Moho depth is certainly underestimated there) and south of the South Baikal basin, in the Hamar-Daban range. Whereas lower crustal thinning is vertically underlying the main active faults of the Centre Baikal basin, it is located ~100 km southward of the Obruchevsky fault, in the South Baikal basin. No active extensional structure exists in the Hamar-Daban range, which means that lower crustal thinning in the South Baikal basin is offset southward with respect to the surface rift axis. Similarly, the surface projection of minimum lithospheric thicknesses does not show any clear correlation with surface structures (Figure 14).

[60] In the South Baikal basin, the main structure accommodating extension is the Obruchevsky fault; this steep, left-lateral normal fault is supposed to branch on ancient steep strike-slip thrusts. No crustal thinning is found beneath the South Baikal basin. Instead, Bouguer gravity anomalies rather advocate for a thick crust. The area of thinner crust lies beneath the high topography of the Hamar-Daban range, suggesting an asymmetry in the rift geometry at depth. Moreover, taking 100–120 km as a transition depth interval from a "normal" to a moderately thinned cratonic lithosphere, we can infer that the southern limit of the Siberian lies almost vertically beneath the South Baikal basin (Figure 14).

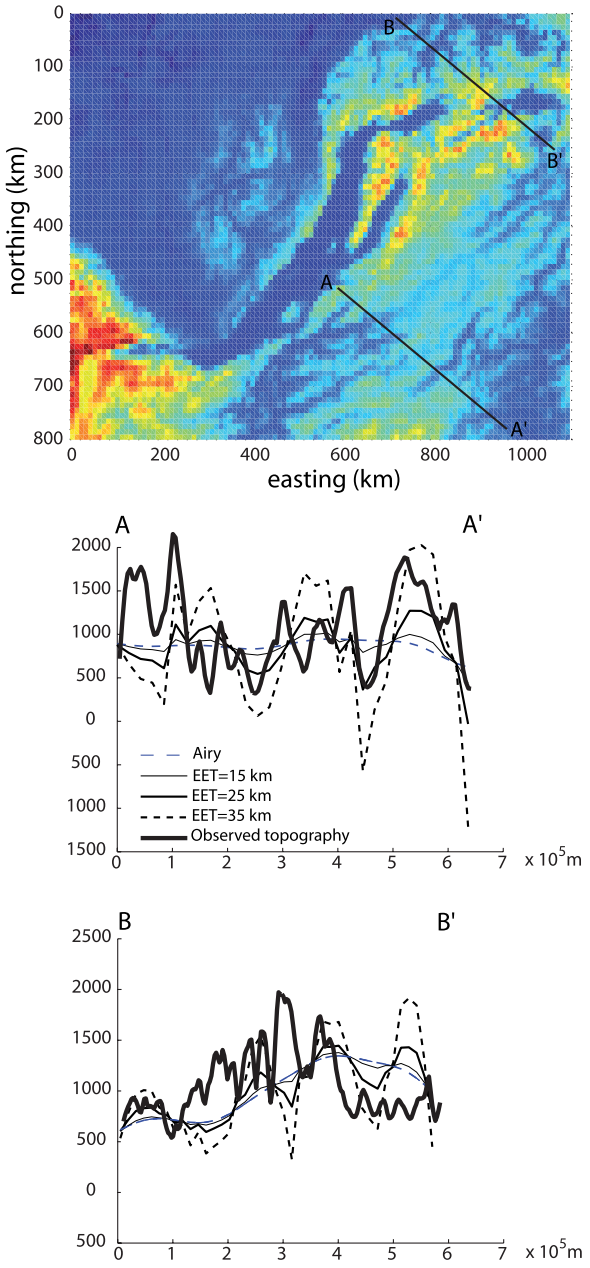

Figure 13. Predicted topography on two NW-SE profiles, based on flexural modeling of the Moho and asthenosphere deflections (see text for explanations). Top panel shows the location of the modeled profiles. Middle and bottom panels show the predicted topography for different values of EET.

[61] On the other hand, the vertical superposition between lower and upper crustal thinning in the Centre Baikal basin suggests more symmetric extension. Two main active faults (the Morsky and Primorsky faults), both dipping SE, could cut across the crust of the Siberian craton, given the maximum earthquake depth of 30 km at this place [*Déverchère et al.*, 2001]. In this region, a thick lithosphere (>100 km) extends well southward of the rift axis, suggesting that the rift faults localize either along inherited low-dipping crustal-scale thrusts following the rim of the craton, or possibly penetrate into the cratonic crust as suggested by *ten Brink and Taylor* [2002] (Figure 14).

[62] From top to bottom, the Baikal rift geometry is thus largely controlled by the presence of the Siberian craton: at the surface, normal faults localize close to the suture and sometimes cut at depth into the cratonic crust. The dip angle of the suture influences not only fault localization and spacing but also the location of lower crustal thinning: when the craton border is steep, a single fault forms along it, and deformation is asymmetric. When the suture dips gently, rift first develops on (or very close to) it (Primorsky fault) and then jumps eastward (Morsky fault), and extension at depth is located beneath the basin. This behavior resembles the "dipping pie" model of *Le Pourhiet et al.* [2004], implying a large or intermediate competence contrast between the suture zone and the rest of the crust.

[63] Actually, fault kinematics should also play an important role in the rift geometry: in the South Baikal rift, opening is oblique so that the Obruchevsky fault has to accommodate an important strike-slip component, whereas extension is almost perpendicular in the Centre Baikal.

5.2. Rift Evolution

[64] We propose in Figure 15 three sketches of the Baikal rift tectonic and magmatic evolution, in the general frame of Asian dynamics. We describe the relative kinematics in a fixed Eurasian plate framework. In this scenario, we clearly favor the role of far-field stresses as the cause of rift opening. We propose it because we think it is a simple model that explains most of the available data exposed above.

[65] From Late Oligocene to Early Miocene (Figure 15a), wide, shallow basins develop along strike-slip faults (Obruchevsky and Morsky in the South and Centre Baikal basins). To the SW, collision between India and Eurasia has started ~30 Ma ago; its first manifestations occur in the Baikal rift through NE-SW horizontal compression. On the eastern margin of the Asian continent, marginal basins (Japan and Okhotsk seas) open in response to Pacific subductions. Ridge push due to the opening of marginal basins are possible sources

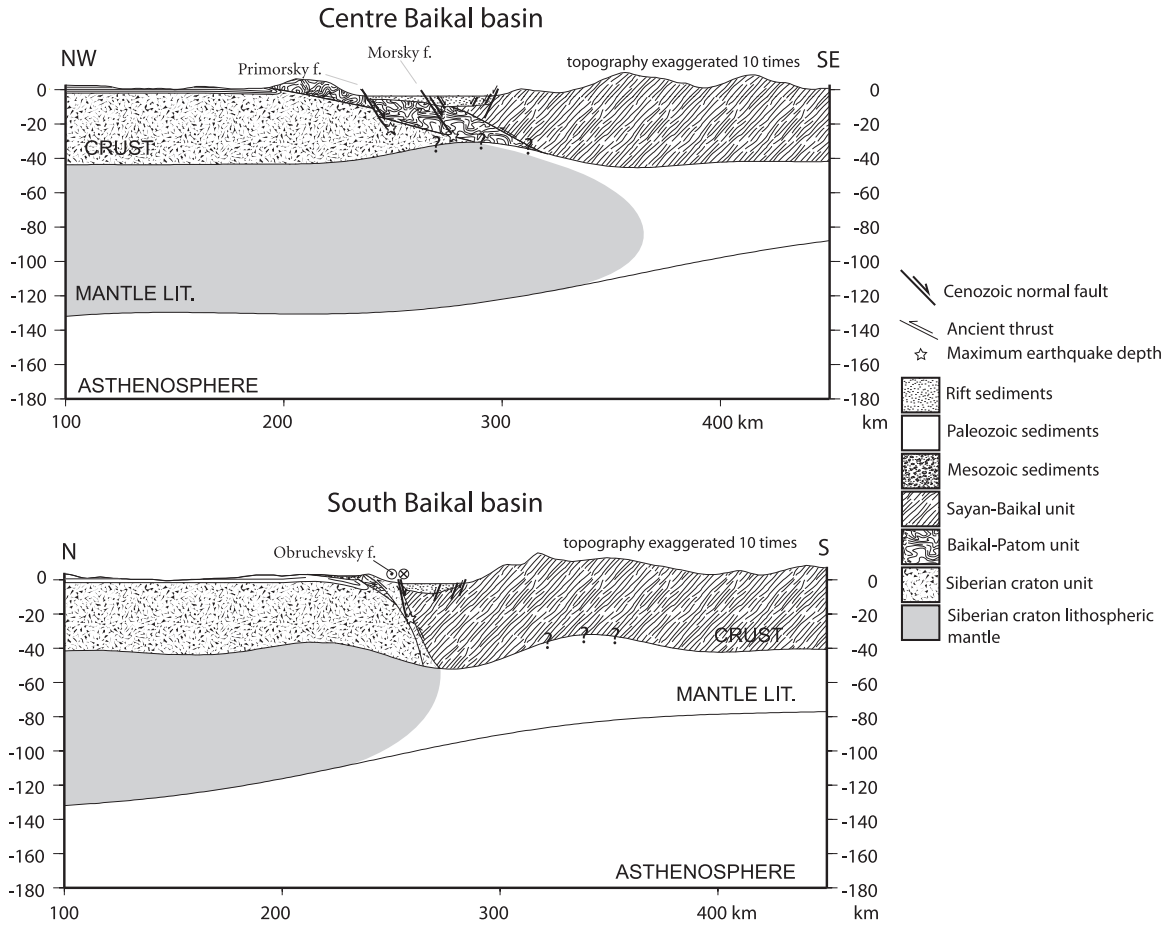

Figure 14. Schematic lithospheric cross sections of the (top) South Baikal and (bottom) Centre Baikal rift zones, based on geological data (Figure 3) and on the inferred Moho and asthenosphere depths (Figures 11 and 12, respectively). See Figure 3 for profile location.

of intraplate compressional stresses counteracting extension in the BRS. Volcanism begins in the Tunka area.

[66] In the Late Miocene, the opening of marginal basins on the Pacific boundary has ceased, which decreases the lateral confining on the eastern boundary of the BRS (Figure 15b). At the same time, N-S to NW-SE compressive body forces due to rapid uplift of the Tibetan plateau combine with compressive stresses coming from the India-Asia collision to increase the level of SW-NE compressive stresses. Rifting is then enabled by the eastward escape of the Amuria-North China plate. In the mantle, magma is generated by decompression melting south and east of the rift axis.

[67] Finally, from Pleistocene to present (Figure 15c), the situation is rather similar except that (1) the continuing penetration of India into Eurasia has increased the level of compressive stresses recorded in the Tunka basin, causing its recent inversion, (2) mantle activity has stopped, and (3) climatic changes are recorded in the sedimentary section.

[68] What do we learn from the example of the Baikal rift? First, its tectonic and magmatic evolutions are echoed in the more general evolution of Asia, to which it belongs, and it makes no sense to separate both of them: indentation of a homogeneous lithosphere would not necessarily create any rift, so India-Asia collision ''needs'' to find a favorably oriented cratonic keel to induce rifting. On the other hand, because of its still thick lithosphere, the Baikal rift has not reached the stage where mantle dynamics is strong enough to maintain extension, and still needs external (even compressive) sources of stress.

[69] Second, there is no single explanation for the origin of the rift, but rather an addition of favorable parameters: plate stresses, large-scale lateral heterogeneities, thermal conditions. Rifting does not necessarily localize where the thermal lithosphere

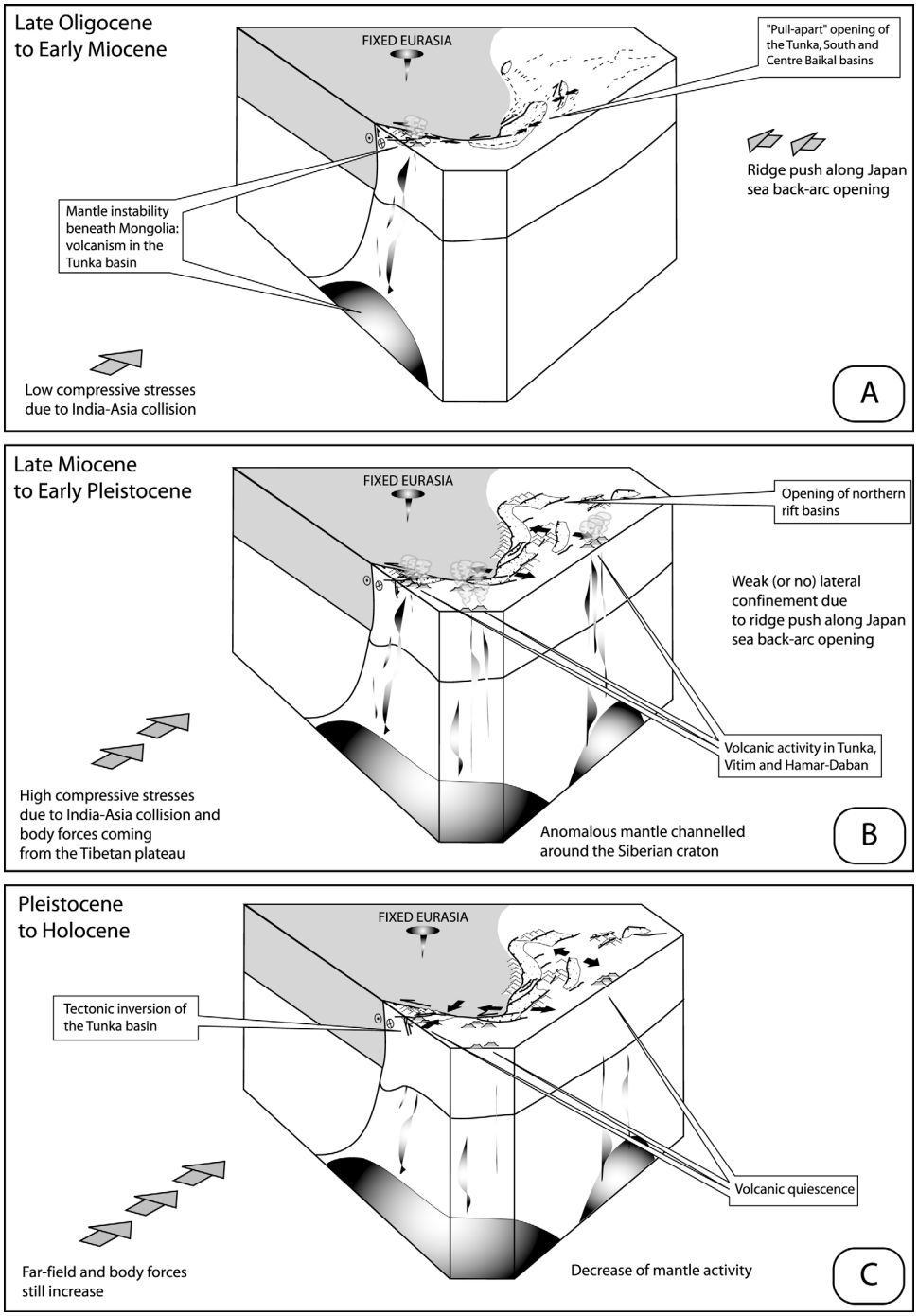

Figure 15. Proposed reconstitution of the tectonic evolution of the BRS.

is thinner, but the inherited thermal and mechanical contrast between the craton and the folded zone is one of the key-factors controlling its development.

[70] Finally, fault geometries and spacing, and topography support change a lot along the strike of the rift; it could be interesting to study how this primitive segmentation controls the geometry of passive margins and the development of transform faults at the onset of oceanic spreading.

Acknowledgments

[71] This paper is the result of a long-lasting collaboration between us and our colleagues and friends from the Institute of the Earth's Crust in Irkutsk. We wish to thank all of them for

their efficiency, warm friendship, and perfect knowledge of their beautiful Siberia. Many of the presented figures owe their existence to the magic power of the Generic Mapping Tools [*Wessel and Smith*, 1991]. We thank C. Ebinger, J. Tarduno (Editor), and an anonymous reviewer for their constructive comments that helped a lot to improve this paper. Number 1008 of the IUEM, European Institute for Marine Studies (Brest, France).

References

Arjannikova, A., C. Larroque, J.-F. Ritz, J. Déverchère, J.-F. Stéphan, S. Arjannikov, and V. A. San'kov (2004), Geometry and kinematics of recent deformation in the Mondy-Tunka area (south-westernmost Baikal rift zone, Mongolia-Siberia), *Terra Nova*, doi:10.1111/j.1365-3121.2004.00565.x.

Ashchepkov, I. V. (1991), *Deep-Seated Xenoliths of the Baikal Rift* (in Russian), 160 pp., Nauka, Novossibirsk, Russia.

Avouac, J.-P., and P. Tapponnier (1993), Kinematic model of active deformation in Central Asia, *Geophys. Res. Lett.*, *20*, 895–898.

Back, S., M. De Batist, M. R. Strecker, and P. Vanhauwaert (1999), Quaternary depositional systems in northern Lake Baikal, Siberia, *J. Geol.*, *107*, 1–12.

Barry, T. L., A. D. Saunders, P. D. Kempton, B. F. Windley, M. S. Pringle, D. Dorjnamjaa, and S. Saandar (2003), Petrogenesis of Cenozoic basalts from Mongolia: Evidence for the role of asthenospheric versus metasomatised mantle sources, *J. Petrol.*, *44*, 55–91.

Brazier, R. A., and A. A. Nyblade (2003), Upper mantle P velocity structure beneath the Baikal Rift from modeling regional seismic data, *Geophys. Res. Lett.*, *30*(4), 1153, doi:10.1029/2002GL016115.

Buck, W. R. (1991), Modes of continental lithospheric extension, *J. Geophys. Res.*, *96*, 20,161–20,178.

Burov, E. B., and M. Diament (1995), The effective elastic thickness (Te) of continental lithosphere: What does it really mean?, *J. Geophys. Res.*, *100*, 3905–3927.

Burov, E., and A. Watts (2005), The long-term strength of continental lithosphere: "Jelly sandwich" or "crème brûlée"?, *GSA Today*, *16*, 4–10.

Burov, E. B., F. Houdry, M. Diament, and J. Déverchère (1994), A broken plate beneath the North Baikal rift zone revealed by gravity modelling, *Geophys. Res. Lett.*, *21*, 129–132.

Calais, E., O. Lesne, J. Déverchère, V. San'kov, A. Lukhnev, A. Miroshnitchenko, V. Buddo, K. Levi, V. Zalutzky, and Y. Bashkuev (1998), Crustal deformation in the Baikal rift from GPS measurements, *Geophys. Res. Lett.*, *25*(21), 4003–4006.

Calais, E., M. Vergnolle, V. San'kov, A. Lukhnev, A. Miroshnitchenko, S. Amarjargal, and J. Déverchère (2003), GPS measurements of crustal deformation in the Baikal-Mongolia area (1994–2002): Implications for current kinematics of Asia, *J. Geophys. Res.*, *108*(B10), 2501, doi:10.1029/2002JB002373.

Chamot-Rooke, N., and X. Le Pichon (1999), GPS determined eastward Sundalan motion with respect to Eurasia confirmed by earthquakes slip vectors at Sunda and Philippine trenches, *Earth Planet. Sci. Lett.*, *173*, 439–455.

Cochran, J. R. (1990), Himalayan uplift, sea level, and the record of Bengal Fan sedimentation at the ODP Leg 116 sites, *Proc. Ocean Drill. Proj. Sci. Results*, *116*, 397–414.

Cunningham, W. D. (2001), Cenozoic normal faulting and regional doming in the southern Hangay region, Central Mongolia: Implications for the origin of the Baikal Rift Province, *Tectonophysics*, *331*, 389–411.

Delouis, B., J. Déverchère, V. Melnikova, N. Radziminovitch, L. Loncke, C. Larroque, J.-F. Ritz, and V. San'kov (2002), A reappraisal of the 1950 (Mw 6.9) Mondy earthquake, Siberia, and its relationship to the strain pattern at the south-western end of the Baikal rift zone, *Terra Nova*, *14*, 491–500.

Delvaux, D., A. Melnikov, and V. D. Ermikov (1995), Paleostress reconstruction and geodynamics of the Baikal region, Central Asia, I, Paleozoic and Mesozoic pre-rift evolution, *Tectonophysics*, *252*, 61–101.

Delvaux, D., R. Moeys, G. Stapel, C. Petit, K. Levi, A. Miroshnichenko, V. Ruzhich, and V. A. San'kov (1997), Paleostress reconstruction and geodynamics of the Baikal region, Central Asia, II, Cenozoic rifting, *Tectonophysics*, *282*, 1–38.

Déverchère, J., F. Houdry, M. Diament, N. V. Solonenko, and A. V. Solonenko (1991), Evidence for a seismogenic upper mantle and lower crust in the Baikal rift, *Geophys. Res. Lett.*, *18*, 1099–1102.

Déverchère, J., F. Houdry, N. V. Solonenko, A. V. Solonenko, and A. V. San'kov (1993), Seismicity, active faults and stress field of the North Muya region, Baikal rift: New insights on the rheology of extended continental lithosphere, *J. Geophys. Res.*, *98*, 19,895–19,912.

Déverchère, J., C. Petit, N. Gileva, N. Radziminovitch, V. Melnikova, and V. San'kov (2001), Depth distribution of earthquakes in the Baikal Rift System and its implications for the rheology of the lithosphere, *Geophys. J. Int.*, *146*, 713–730.

Doser, D. I. (1991a), Faulting within the western Baikal rift as characterized by earthquake studies, *Tectonophysics*, *196*, 87–107.

Doser, D. I. (1991b), Faulting within the eastern Baikal rift as characterized by earthquake studies, *Tectonophyiscs*, *196*, 109–139.

Ermikov, V. D. (1994), Mesozoic precursors of the Cenozoic rift structures of Central Asia, *Bull. Cent. Rech. Explor. Prod. Elf-Aquitaine*, *18*, 123–134.

Fournier, M., L. Jolivet, P. Huchon, V. S. Rozhdestvensky, K. F. Sergeyev, and L. Oscorbin (1994), Neogene strike-slip faulting in Sakhalin, and the Japan Sea opening, *J. Geophys. Res.*, *99*, 2701–2725.

Fournier, M., L. Jolivet, P. Davy, and J. C. Thomas (2004), Backarc extension and collision: An experimental approach to the tectonics of Asia, *Geophys. J. Int.*, *157*, 871–889.

Gao, S. S., K. H. Liu, P. M. Davis, P. D. Slack, Y. A. Zorin, V. V. Mordvinova, and V. M. Kozhevnikov (2003), Evidence for small-scale mantle convection in the upper mantle beneath the Baikal rift zone, *J. Geophys. Res.*, *108*(B4), 2194, doi:10.1029/2002JB002039.

Gao, S. S., K. H. Liu, and C. Chen (2004), Significant crustal thinning beneath the Baikal rift zone: New constraints from receiver function analysis, *Geophys. Res. Lett.*, *31*, L20610, doi:10.1029/2004GL020813.

Golubev, V. A. (2000), Conductive and convective heat flow in the bottom of Lake Baikal and in the surrounding mountains, *Bull. Cent. Rech. Explor. Prod. Elf-Aquitaine*, *22*, 323–340.

Harrison, T. M., P. Copeland, W. S. F. Kidd, and A. Yin (1992), Raising Tibet, *Science*, *255*, 1663–1670.

Houdry, F. (1994), Mécanismes de l'extension continentale dans le rift Nord-Baïkal, Sibérie: Contraintes des données d'imagerie SPOT, de terrain, de sismologie et de gravimétrie, Ph.D. thesis, 345 pp., Univ. Pierre et Marie Curie, Paris.

Hutchinson, D. R., A. J. Golmshtok, L. P. Zonenshain, T. C. Moore, C. A. Scholtz, and K. D. Klitgord (1992), Depositional and tectonic framework of the rift basins of Lake Baikal from multichannel seismic data, *Geology*, *20*, 589–592.

INTAS Project 99-1669 Team (2002), A new bathymetric map of Lake Baikal, Open-File Report on CD-ROM, Gent, Belgium.

Ionov, D. (2002), Mantle structure and rifting processes in the Baikal-Mongolia region: Geophysical data and evidence from xenoliths in volcanic rocks, *Tectonophysics*, *351*, 41–60.

Ionov, D. A., S. Y. O'Reilly, and I. V. Ashchepkov (1995), Feldspar-bearing lherzolite xenoliths in alkali basalts from Hamar-Daban, southern Baikal region, Russia, *Contrib. Mineral. Petrol.*, *122*, 174–190.

Ivanov, A. V. (2004), One rift, two models, *Sci. First Hand*, *1*, 50–62.

Jolivet, L., and K. Tamaki (1992), Neogene kinematics in the Japan Sea region and the volcanic activity of the Northeast Japan arc, *Proc. Ocean Drill. Program Sci. Results*, *127/128*, 1311–1331.

Kashik, S. A., and V. N. Masilov (1994), Main stages and palaeogeography of Cenozoic sedimentation in the Baikal rift system (eastern Siberia), *Bull. Cent. Rech. Explor. Prod. Elf-Aquitaine*, *18*, 453–461.

Kiselev, A. I., and A. M. Popov (1992), Asthenospheric diapir beneath the Baikal rift: Petrological constraints, *Tectonophysics*, *208*, 287–295.

Kiselev, A. I., H. A. Golovko, and M. E. Medvedev (1978), Petrochemistry of Cenozoic basalts and associated rocks in the Baikal rift zone, *Tectonophysics*, *45*, 49–59.

Kooi, H., S. Cloetingh, and J. Burrus (1992), Lithospheric necking and regional isostasy at extensional basins: 1. Subsidence and gravity modeling with an application to the Gulf of Lions Margin (SE France), *J. Geophys. Res.*, *97*, 17,553–17,571.

Kuzmin, M. I., E. B. Karabanov, A. A. Prokopenko, V. F. Gelety, V. S. Antipin, D. F. Williams, and A. N. Gvozdkov (2000), Sedimentation processes and new age constraints on rifting stages in Lake Baikal: Results of deep-water drilling, *Int. J. Earth. Sci.*, *89*, 183–192.

Larroque, C., J.-F. Ritz, J.-F. Stéphan, V. A. San'kov, A. Arjannikova, E. Calais, J. Déverchère, and L. Loncke (2001), Interaction compression-extension à la limite Mongolie-Sibérie: Analyse préliminaire des déformations récentes et actuelles dans le bassin de Tunka, *C. R. Acad. Sci. Paris*, *332*, 177–184.

Le Pourhiet, L., E. Burov, and I. Moretti (2004), Rifting through a stack of inhomogeneous thrusts (the dipping pie concept), *Tectonics*, *23*, TC4005, doi:10.1029/2003TC001584.

Lesne, O., E. Calais, and J. Deverchère (1998), Finite element modeling of present-day kinematics and strain in the Baikal rift zone, Siberia, *Tectonophysics*, *289*, 327–430.

Levi, K., A. I. Miroshnichenko, V. A. San'kov, S. M. Babushkin, G. V. Larkin, A. A. Badardinov, H. K. Wong, S. Colman, and D. Delvaux (1997), Active faults of the Baikal depression, *Bull. Cent. Rech. Explor. Prod. Elf-Aquitaine*, *21*, 399–434.

Logatchev, N. A., and N. A. Florensov (1978), The Baikal system of rift valleys, *Tectonophysics*, *45*, 1–13.

Logatchev, N. A., and Y. A. Zorin (1987), Evidence and causes for the two-stage development of the Baikal rift, *Tectonophysics*, *143*, 225–234.

Logatchev, N. A., and Y. A. Zorin (1992), Baikal rift zone: Structure and geodynamics, *Tectonophysics*, *208*, 273–286.

Lysak, S. V. (1978), The Baikal rift heat flow, *Tectonophysics*, *45*, 87–93.

Lysak, S. V. (1984), Terrestrial heat flow in the south of East Siberia, *Tectonophysics*, *103*, 205–215.

Mats, V. D. (1993), The structure and development of the Baikal rift depression, *Earth Sci. Rev.*, *34*, 81–118.

Mats, V. D., O. M. Khlystov, M. De Batist, S. Ceramicola, T. K. Lomonosova, and A. Klimansky (2000), Evolution of the Academician ridge accommodation zone in the central part of the Baikal rift, from high-resolution reflection seismic profiling and geological field investigations, *Int. J. Earth Sci.*, *89*, 229–250.

McKenzie, D. P., and D. Fairhead (1997), Estimates of the effective elastic thickness of the continental lithosphere from Bouguer and free-air gravity anomalies, *J. Geophys. Res.*, *102*, 27,523–27,552.

Melnikov, A. I., A. M. Mazukabzov, E. V. Sklyarov, and E. P. Vasiliev (1994), Baikal rift basement: Structure and tectonic evolution, *Bull. Cent. Rech. Explor. Prod. Elf-Aquitaine*, *18*, 99–122.

Molnar, P. (2005), Mio-Pliocene growth of the Tibetan Plateau and evolution of East Asian climate, *Palaeontol. Electron.*, *8*(1), 23 pp. (Available at http://palaeo-electronica.org/paleo/2005_1/molnar2/issue1_05.htm)

Molnar, P., and P. Tapponnier (1975), Cenozoic tectonics of Asia: Effects of a continental collision, *Science*, *189*, 419–426.

Moore, T. C., K. D. Klitgord, A. J. Golmshtok, and E. Weber (1997), Sedimentation and subsidence patterns in the central and north basins of Lake Baikal from seismic stratigraphy, *Geol. Soc. Am. Bull.*, *109*, 746–766.

Nikolaev, V. G., L. A. Vanyakin, V. V. Kalinin, and V. Y. Milanovskiy (1985), The sedimentary section beneath Lake Baikal, *Int. Geol. Rev.*, *27*, 449–459.

Parfenov, L. M., B. M. Koz'min, V. S. Imayev, and L. A. Savostin (1987), The tectonic character of the Olekma-Stanovoy seismic zone, *Geotectonics*, *21*, 560–572.

Pavlenkova, G. A., K. Priestley, and J. Cipar (2002), 2D model of the crust and uppermost mantle along rift profile, Siberian craton, *Tectonophysics*, *355*, 171–186.

Petit, C., J. Déverchère, F. Houdry, V. A. San'kov, V. I. Melnikova, and D. Delvaux (1996), Present-day stress field changes along the Baikal rift and tectonic implications, *Tectonics*, *15*, 1171–1191.

Petit, C., E. B. Burov, and J. Déverchère (1997), On the structure and mechanical behavior of the extending lithosphere in the Baikal rift from gravity modelling, *Earth Planet. Sci. Lett.*, *149*, 29–42.

Petit, C., I. Koulakov, and J. Déverchère (1998), Velocity structure around the Baikal rift from teleseismic and local earthquake traveltimes and geodynamic implications, *Tectonophysics*, *296*, 125–144.

Petit, C., J. Déverchère, E. Calais, V. A. San'kov, and D. Fairhead (2002), Deep structure and mechanical behavior of the lithosphere in the Hangai-Hövsgöl region, Mongolia: New constraints from gravity modeling, *Earth Planet. Sci. Lett.*, *197*, 133–149.

Pollack, H. N., S. J. Hurter, and J. R. Johnson (1993), Heat flow from the Earth's interior: Analysis of the global data set, *Rev. Geophys.*, *31*, 267–280.

Poort, J., and J. Klerkx (2004), Absence of a regional surface thermal high in the Baikal rift: New insights from detailed contouring of heat flow anomalies, *Tectonophysics*, *383*, 217–241.

Radziminovitch, N., J. Déverchère, V. Melnikova, V. A. San'kov, and N. Giljova (2005), The 1999 Mw 6.0 earthquake sequence

in the Southern Baikal rift, Asia, and its seismotectonic implications, *Geophys. J. Int.*, *161*, 387–400.

Rasskasov, S. V. (1994), Magmatism related to the East Siberia rift system and the geodynamics, *Bull. Cent. Rech. Explor. Prod. Elf-Aquitaine*, *18*, 437–452.

Rasskasov, S. V., et al. (2002), Late Cenozoic volcanism in the Baikal Rift System: Evidence for formation of the Baikal and Khubsugul Basins due to thermal impacts on the lithosphere and collision-derived tectonic stress paper presented at SIAL III: The Third International Symposium on Speciation in Ancient Lakes, Russ. Acad. of Sci., Irkutsk, Russia, 2–7 Sept.

Ruppel, C. (1995), Extensional processes in continental lithosphere, *J. Geophys. Res.*, *100*, 24,187–24,215.

Ruppel, C., M. G. Kogan, and M. K. McNutt (1993), Implications of new gravity data for the Baikal rift zone structure, *Geophys. Res. Lett.*, *20*, 1635–1638.

Sankov, V., J. Déverchère, Y. Gaudemer, F. Houdry, and A. Filippov (2000), Geometry and rate of faulting in the North Baikal rift, Siberia, *Tectonics*, *19*, 707–722.

Scholz, C. A., and D. R. Hutchinson (2000), Stratigraphic and structural evolution of the Selenga delta accommodation zone, Lake Baikal rift, Siberia, *Int. J. Earth Sci.*, *89*, 212–228.

Sengör, A. M. C., and K. Burke (1978), Relative timing of rifting and volcanism on Earth and its tectonic implications, *Geophys. Res. Lett.*, *5*, 419–421.

Shapiro, N. M., and M. H. Ritzwoller (2002), Monte-Carlo inversion for a global shear-velocity model of the crust and upper mantle, *Geophys. J. Int.*, *151*, 88–105.

Sherman, S. I. (1992), Fault and tectonic stresses of the Baikal rift zone, *Tectonophysics*, *208*, 297–307.

Sherman, S. I., V. M. Dem'Yanovich, and S. V. Lysak (2004), Active faults, seismicity and recent fracturing in the lithosphere of the Baikal rift system, *Tectonophysics*, *380*, 261–272.

Sleep, N. H. (1996), Lateral flow of plume material ponded at sublithospheric depths, *J. Geophys. Res.*, *101*, 28,065–28,083.

Suvorov, V. D., Z. M. Mishenkina, G. V. Petrick, I. F. Sheludko, V. S. Seleznev, and V. M. Solovyov (2002), Structure of the crust in the Baikal Rift Zone and adjacent areas from Deep Seismic Sounding data, *Tectonophysics*, *351*, 61–74.

Tapponnier, P., and P. Molnar (1979), Active faulting and Cenozoic tectonics of the Tien Shan, Mongolia and Baykal regions, *J. Geophys. Res.*, *84*, 3425–3455.

ten Brink, U. S., and M. H. Taylor (2002), Crustal structure of central Lake Baikal: Insights into intracontinental rifting, *J. Geophys. Res.*, *107*(B7), 2132, doi:10.1029/2001JB000300.

Tiberi, C., M. Diament, J. Déverchère, C. Petit-Mariani, V. Mikhailov, S. Tikhotsky, and U. Achauer (2003), Deep structure of the Baikal rift zone revealed by joint inversion of gravity and seismology, *J. Geophys. Res.*, *108*(B3), 2133, doi:10.1029/2002JB001880.

van der Beek, P. (1997), Flank uplift and topography at the Central Baikal rift (SE Siberia): A test of kinematic models for continental extension, *Tectonics*, *16*, 122–136.

van der Beek, P., D. Delvaux, P. A. M. Andriessen, and K. G. Levi (1999), Early cretaceous denudation related to convergent tectonics in the Baikal region, SE Siberia, *J. Geol. Soc. London*, *153*, 515–523.

Villaseñor, A., M. H. Ritzwoller, A. L. Levshin, M. P. Barmin, E. R. Engdahl, W. Spakman, and J. Trampert (2001), Shear velocity structure of central Eurasia from inversion of surface wave velocities, *Phys. Earth Planet. Inter.*, *123*, 169–184.

Wang, J.-H., A. Yin, T. M. Harrison, M. Grove, Y.-Q. Zhang, and G.-H. Xie (2001), A tectonic model for Cenozoic igneous activities in the Eastern Indo-Asian collision zone, *Earth Planet. Sci. Lett.*, *188*, 123–133.

Watts, A. B., and E. V. Burov (2003), Lithospheric strength and its relationship to the elastic and seismogenic layer thickness, *Earth Planet. Sci. Lett.*, *213*, 113–131.

Wei, D.-P., and T. Seno (1998), Determination of the Amurian plate motion, in *Mantle Dynamics and Plate Interactions in East Asia*, *Geodyn. Ser.*, vol. 27, edited by M. Flower et al., pp. 337–346, AGU, Washington D. C.

Wessel, P., and W. H. F. Smith (1991), Free software helps map and display data, *Eos Trans. AGU*, *72*, 441.

Windley, B. F., and M. B. Allen (1993), Mongolia plateau: Evidence for a late Cenozoic mantle plume beneath central Asia, *Geology*, *21*, 295–298.

Wu, F. T., A. L. Levshin, and V. M. Kozhevnikov (1997), Rayleigh wave group velocity tomography of Siberia, China, and the vicinity, *Pure Appl. Geophys.*, *149*, 447–473.

Yanovskaya, T. B., and V. M. Kozhevnikov (2003), 3D S-wave velocity pattern in the upper mantle beneath the continent of Asia from Rayleigh wave data, *Phys. Earth Planet. Inter.*, *138*, 263–278.

Zonenshain, L. P., and L. A. Savostin (1981), Geodynamics of Baikal rift zone and plate tectonics of Asia, *Tectonophysics*, *76*, 1–45.

Zorin, Y. A. (1981), The Baikal rift: An example of the intrusion of asthenospheric material into the lithosphere as the cause of disruption of lithospheric plates, *Tectonophysics*, *73*, 91–104.

Zorin, Y. A. (1999), Geodynamics of the western part of the Mongolia-Okhotsk collisional belt, Trans-Baikal region (Russia) and Mongolia, *Tectonophysics*, *306*, 33–56.

Zorin, Y. A., V. M. Kozhevnikov, M. R. Novoselova, and E. K. Turutanov (1990), Structure of the lithosphere of the Mongolian-Siberian mountainous province, *J. Geodyn.*, *11*, 327–342.

Zorin, Y. A., V. V. Mordvinova, E. K. Turutanov, B. G. Belichenko, A. A. Artemyev, G. L. Kosarev, and S. S. Gao (2002), Low seismic velocity layers in the Earth's crust beneath Eastern Siberia (Russia) and Central Mongolia: Receiver function data and their possible geological implication, *Tectonophysics*, *359*, 307–327.